What are HI profiles of cluster galaxies telling us?

Hugo Silva,
Mestrado em Astronomia e Astrofísica
Departamento de Física e Astronomia
2020

Orientador
Dr. Tom Scott, Faculdade de Ciências

Coorientador
Prof. Dr. Catarina Lobo Faculdade Ciências

U.PORTO

FACULDADE DE CIÊNCIAS
UNIVERSIDADE DO PORTO

Todas as correções determinadas pelo júri, e só essas, foram efetuadas.

O Presidente do Júri,

Porto, _____/_____/_____

Universidade do Porto

Masters Thesis

What are HI profiles of cluster galaxies telling us?

Author:
Hugo Silva

Supervisor:
Tom Scott

Co-supervisor:
Catarina Lobo

A thesis submitted in fulfilment of the requirements
for the degree of MSc. in Astronomy and Astrophysics

at the

Faculdade de Ciências da Universidade do Porto
Departamento de Física e Astronomia

December 29, 2020

Acknowledgements

This journey would not have been possible without the support of numerous people. My supervisor, Tom Scott, and co-supervisor, Catarina Lobo, have provided indescribable help and encouragement throughout my work on this thesis. I give them my most sincere thank you and truly appreciate their generosity with time and patience.

I also need to thank my family, who has been tremendously important during the last year, providing a haven I could turn to whenever necessary.

Lastly, I must thank my girlfriend, Sofia, who was always ready to help me with whatever I needed and was able to be there for me, even though we were far apart. Thank you.

UNIVERSIDADE DO PORTO

Abstract

Faculdade de Ciências da Universidade do Porto

Departamento de Física e Astronomia

MSc. in Astronomy and Astrophysics

What are HI profiles of cluster galaxies telling us?

by Hugo Silva

A262 is a spiral rich galaxy cluster with low redshift(z=0.01742), it's a good contender to study HI profiles from its galaxies because of it's low redshift and availability of integrated HI spectra. HI is usually preferentially stripped from the outer part of the disks by processes attributable to the cluster environment, such as ram pressure stripping or tidal stripping. This often results in galaxies with a deficiency of HI, having smaller HI disks, which has an impact on the star formation rate - with a possible temporary increase of the quenching of starformation.

In this project, we look for signatures of the effects of the cluster environment on the abundance and distribution of HI as well as it's impact on starformation. Studying the integrated HI and selected stellar properties gives a view of what happened to the galaxy, potentially enabling us to disentangle the cause (hydrodynamical effects versus tidal ones). Our sample consists of 30 galaxies from the cluster A262 with single dish HI detections. We studied the relations between the star-formation rate and stellar mass, the HI deficiency and HI profile asymmetry. We also looked for a relation between the galaxies position inside the cluster and their HI and stellar properties.

Statistically significant relations were found between the HI deficiency and projected distance to the cluster center, HI mass and star formation rate. The HI mass and baryonic mass have a correlation with the rotational velocity of the galaxy, confirming the Tully-Fisher and the baryonic Tully-Fisher relations for this cluster, with a smaller correlation for the baryonic Tully-Fisher relation most likely due to interactions with the cluster environment which might cause this divergence. There was also found correlation between the HI mass and the SFR as expected.

Finally we analysed galaxies with the most extreme properties in our sample, i.e. A_{flux}, HI deficiency and SFR. For these galaxies we tried to determine the most likely mechanism causing these signatures. From this analysis we found evidence of a mix of ram pressure and tidal mechanism both past and ongoing.

Keywords - galaxies: clusters: intracluster medium, galaxies: clusters: individual: Abell262

UNIVERSIDADE DO PORTO

Resumo

Faculdade de Ciências da Universidade do Porto

Departamento de Física e Astronomia

Mestrado em Astronomia e Astrofísica

O que estão os perfis de HI das galáxias em enxame a contar-nos?

por Hugo Silva

A262 é um enxame de galáxias rico em espirais com redshift baixo(z = 0,01742) este enxame é um bom candidato para estudar perfis de HI das suas galáxias devido ao seu baixo redshift e à disponibilidade do espectro integrado de HI. Geralmente HI é preferencialmente removido da parte externa dos discos por processos causados pelo ambiente interno do enxame, como remoção de gás através de ram pressure ou efeitos de maré. Isto frequentemente resulta em galáxias com deficiência de HI terem discos de HI menores que tem impacto na taxa de formação estelar - que temporariamente pode aumentar a taxa de formação de estrelas. Neste projecto, procuramos assinaturas dos efeitos que o ambiente do enxame tem na abundância, distribuição e o impacto na formação estelar que o HI tem. O estudo do HI integrado e das propriedades estelares selecionadas, potencialmente permite uma visão do que aconteceu com a galáxia(processos hydrodinâmicos ou efeitos de maré). A nossa amostra consiste em 30 galáxias do enxame A262 com detecções HI de single-dish. Nós estudamos as relações entre a taxa de formação de estrelar e a massa estelar, a deficiência de HI e o perfil de HI. Também procuramos uma relação entre a posição das galáxias dentro do aglomerado e suas propriedades, HI deficiency e parametros estelares. Relações estatisticamente significativas foram encontradas entre a deficiência de HI com a distância ao centro do enxame, a massa de HI e a taxa de formação de estrelar. A massa de HI e a massa bariônica têm uma correlação com a velocidade rotacional das galáxias, confirmando as relações tully-fisher para este enxame, com uma correlação menor para a relação de Tully-Fisher bariônica provavelmente devido a interacções com o ambiente do enxame que podem ter causado esta divergência. Também foi encontrado uma correlação entre a massa de HI com a taxa de formação estelar como seria esperado. Finalmente

analisamos as galáxias com as propriedades mais notáveis na nossa amostra, i.e. A_{flux}, HI deficiency e taxa de formação estelar. Para estas galáxias tentamos determinar os mecanismos que podem ter causado estas assinaturas. Desta análise descobrimos uma mistura de ram pressure e forças de maré ambos no passado como no presente.

Palavras-chave - galáxias: enxames: meio inter-enxame, galáxias: enxame: individual: Abell262

Contents

List of Figures

Chapter 1

Introduction

1.1 Galaxy clusters

Most galaxies belong to groups or clusters. Clusters and groups are structures where galaxies are gravitationally bound to the cluster or group's gravitational potential and orbit the center of mass.

Poor clusters contain approximately 50 galaxies while rich clusters may contain thousands of galaxies with a radii up to 4000 kpc. The velocity dispersion of clusters is typically $\sim$ 800 km s^{-1} and can surpass 1000 km s^{-1} for very rich clusters, with a mass of the order of $10^{15} M_{\odot}$, Kravtsov & Borgani(2012). In general, groups contain less than 50 galaxies, a radius of $\sim 500 kpc$ and have a total mass in the order of $10^{13} M_{\odot}$, Román & Trujillo(2017).

The gravity of the cluster is strong enough to dominate over the expansion of the universe so objects within the cluster remain gravitationally bound to the cluster while the universe as a whole keeps expanding. The mass content of clusters is typically 90% for dark matter, the hot (10^7 K) X-ray emitting intracluster medium (ICM) corresponds to 9% and the gas and stars in galaxies correspond to 1% of the cluster mass. With HI making up approximately 10 % of the galaxies baryonic mass

Dark matter is the predominant component in the cluster and due to its effect on the ICM, the ICM density is highest at the cluster centre and falls systematically toward the outskirts of the cluster. The Bullet cluster is one of the more conclusive proofs of the existence of dark matter, see Figure 1.1. This cluster consists of two clusters of galaxies colliding but the principal components behave very differently: the galaxies remain bound to the dark matter during the interaction. The dark matter was detected using gravitational lensing of the objects beyond the cluster. Since the gravitational lensing cannot

be explained with the baryonic matter, it leaves the dark matter as the only explanation for this behavior. Dark matter that doesn't emit light but has a gravitational impact on baryonic matter. The interaction between two clusters in figure 1.1 illustrates how each cluster's galaxies are bound to the two dark matter halos (green contours) during the interaction. In contrast, the X-ray emitting ICM(colour in the right panel of Figure 1.1) has temporarily been removed from the dark matter halo because of a collisional interaction.

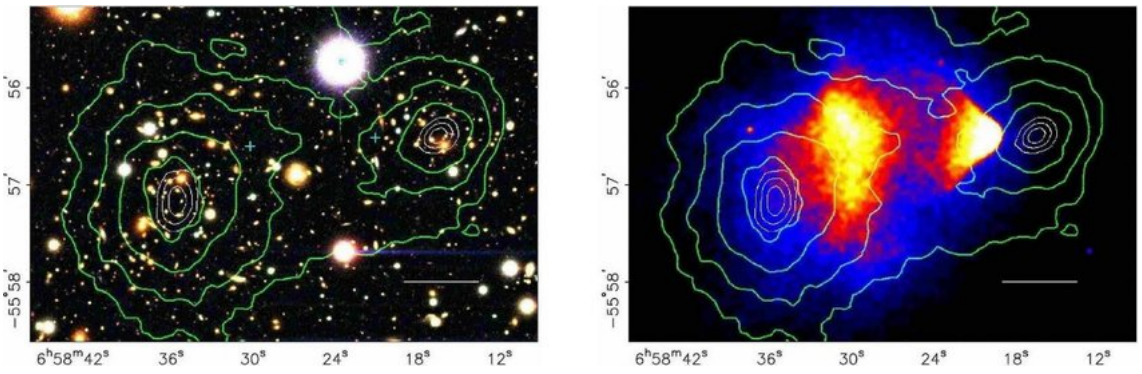

Figure 1.1: Bullet cluster. The interaction between two clusters in the figure illustrates how each cluster's galaxies are bound to their dark matter halos(green contours) during the interaction. In this case the X-ray emitting ICM it has temporarily been removed from the both of dark matter potentials because of collisional interactions between the gas particles. Left image shows the optical image from the bullet cluster and the right image shows the displaced X-ray from the gas Clowe et al.(2006)

The virial radius (R_{vir}) of a cluster is defined by the radius within which the system is in equilibrium and beyond which the mass is still collapsing into the cluster. R_{vir} can be computed using equation from Lewis et al.(2002):

$$R_{vir} = 3.5\sigma(1+z)^{-1.5} \tag{1.1}$$

Where R_{vir} is the virial radius in Mpc, σ the velocity dispersion of the cluster in units of 1000 km/s and z the redshift of the cluster.

Looking at the relation between the virial radius and the X-ray luminosity we to see where A262 fits in comparison to the other nearby Abell clusters. In figure 1.2, we take a sample of 137 Abell clusters with a computed virial radius using equation 1.1 and the X-ray luminosity obtained from Plionis & Tovmassian(2003) and Wu et al. (1998). We see that the X-ray luminosity tends to increase with the increase in the R_{vir} of the cluster but with significant scatter.

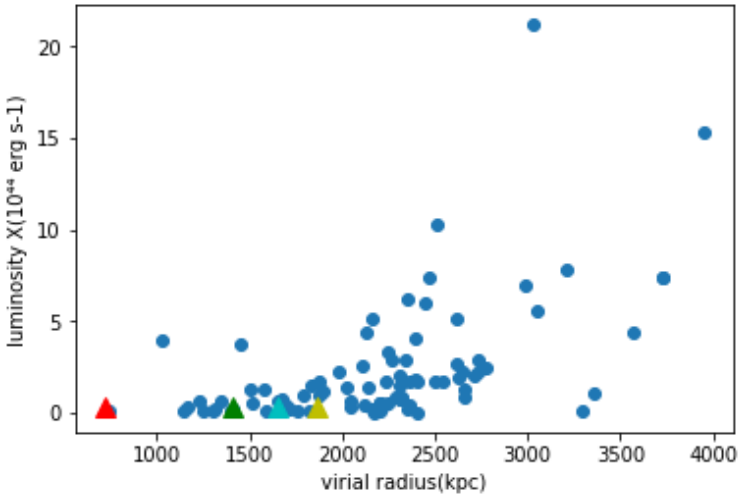

Figure 1.2: Plot of the X-ray luminosity for the Abell clusters as function of their virial radius from Plionis & Tovmassian(2003) and Wu et al. (1998) shown with blue dots. The Red triangle is the virial radius of A262 calculated from the Hassan et al.(2016) velocity dispersion and the green triangle is the 2σ of their velocity dispersion. The yellow triangle is the *R_vir* based on the velocity dispersion from Neill et al. (2001) and the cyan triangle is the average low-velocity dispersion of clusters in the richness class 0 from Fadda et al. (1996)

1.2 Abell 262

Abell 262 is a galaxy cluster that belongs to the Perseus-Pisces supercluster.

Hassan et al.(2016) gives a right ascension of 01h52m50.4s, a declination of +36”08’46, R_{vir} of 35 arcmin, a radial velocity of 4852+-22 kms^{-1} and a velocity dispersion of 212kms^{-1} for the cluster. The distance to the cluster from NED is 75.38 ± 5.41 Mpc. William Herschel, the first observer of this cluster, discovered four galaxies in the central region*. Today, around 100 galaxies of Abell 262 are cataloged in the Catalog of Galaxies and Clusters of Galaxies (CGCG) and many of the spiral galaxies are cataloged in the Uppsala General Catalog of Galaxies (UGC) that holds information like magnitude and galaxies type (see figure 1.3). The richness of a cluster is defined by the number of galaxies in that cluster. Abell 262 is a poor, not very massive cluster that belongs to group 0 of richness. This is consistent with a low velocity dispersion which is related to the cluster’s total mass. The Bautz-Morgan classification is a system for clusters based on the degree in which the cluster is dominated by the brightest galaxies. Type I clusters have a central cD galaxy, type II contain a normal giant elliptical galaxy at their center, and type III doesn’t have a dominant galaxy. Abell 262 has a Bautz-Morgan classification of III.

*https://www.astronomy-mall.com/Adventures.In.Deep.Space/agc262ch.htm

The velocity dispersion obtained by Hassan et al.(2016) was σ=212 kms^{-1}. The virial radius R_{vir}=722.78 kpc from Equation 1.1 using the velocity dispersion given in Hassan et al.(2016) indicate a smaller cluster compared to typical clusters in the sample, in figure 1.2. To explore beyond the virial radius and to compensate the uncertainties when calculating the true R_{vir}, we considered galaxies within a radius based on two times the Hassan velocity dispersion in our HI sample.

The velocity dispersion of 548 obtained by Neill et al. (2001) is calculated from a sample of 101 galaxies in A262 and applying equation 1.1 gives a virial radius R_{vir}=18698 kpc. The velocity dispersion of 485 kms^{-1} obtained by Fadda et al. (1996) is the average low-velocity dispersion of clusters in the richness class 0 and, applying equation 1.1, gives a R_{vir}=1654. Hassan did an analysis on 55 galaxies. With the Hassan virial radius, we get a very small cluster with most of the galaxies of our sample outside the 2 times the Hassan virial radius. The spacial scale for galaxies in the cluster from NED is 21.93 kpc/arcmin.

Figure 1.3: Abell 262: optical image of the central region*

*http://www.jburnell.com/Abell262.html

1.3 HI

Atomic hydrogen is the principal component in the interstellar medium of late type galaxies, being the underlying fuel for star formation. In isolated galaxies the HI gas disk is much bigger than the optical disk: roughly 1.8 times the optical diameter and a flatish radial distribution with sometimes a central hole, the thickness of the HI disk is larger to the optical thickness of the disk, Broeils A. H. et al. 1997. The HI in the outer HI disk is not strongly bound by the galaxy's gravitational potential and can be easily removed from the galaxy by interactions. Because of this, the mass of HI and its distribution is expected can be very different between isolated galaxies and the ones inside clusters because of the impact of interactions with the cluster environment. The distribution of star formation inside the galaxies is more concentrated in regions with higher HI column densities, Kennicutt, Robert C. (1998) and many spiral galaxies don't have axisymmetric distribution in their HI, Jog et al. (2008). The influence of the environment is the most important factor on the HI distribution inside the galaxy and this distribution can reflect the impact of the gas removal mechanisms such as ram pressure stripping and tidal forces.

Neutral atomic hydrogen is typically abundant in the interstellar medium of galaxies and emits at a wavelength of 21 cm. Analyzing HI velocity profiles of the galaxies, we can detect the effects that the cluster environment (ram pressure and tidal force) is currently having on the HI disks of late-type galaxies. The neutral hydrogen atoms emission is detectable at $\lambda = 21$ cm from the hyperfine line. This line results from a drop in the energy level of the atoms caused by the interaction between the electron spin which and the nuclear spin causes the emission of a photon with a wavelength of $\lambda = 21$ cm, see figure 1.4. The HI gas is more abundant in spiral galaxies than in earlier Hubble types. Cold HI clouds emit a radio emission line with a wavelength of 21 cm. Because of the recessional velocity of the galaxy and Doppler shifts from the motion of gas within the galaxy's HI disk, the emission line will be redshifted and spread over a range of velocities.

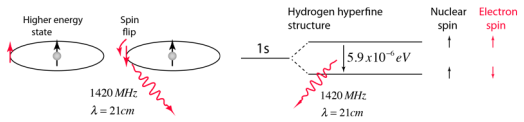

Figure 1.4: Illustrations of the hyperfine spin flip transition of the hydrogen atom and release of a 21cm photon. Credit to Hyperphysics

In this project, we are using single-dish observations from the Arecibo observatory which has no spatial resolution for A262 galaxies because of its 3.5 arcmin beam, so we only have resolution in velocity. The single-dish HI data allows a better understanding of the relation between the HI and stellar properties, Wang et al.(2017).

The inclination of a galaxy's HI disk impacts the observed HI profile with a double horn HI profile, indicating an edge-on rotating HI disk. A single spike HI profile implies a face-on HI disk (see images 1.5 and 1.6).

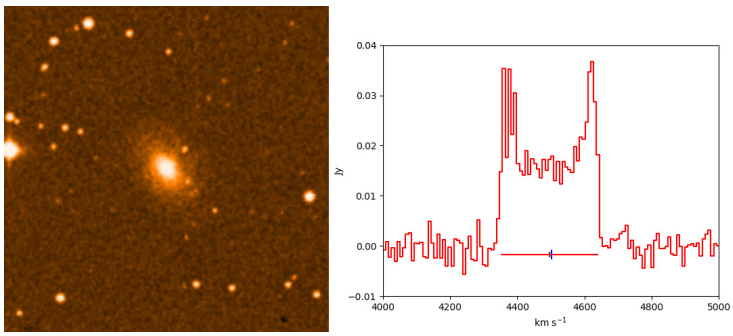

Figure 1.5: Example of the HI profile obtained for a Edge-on galaxy (CGCG 522-001) with optical inclination=44.69 degrees

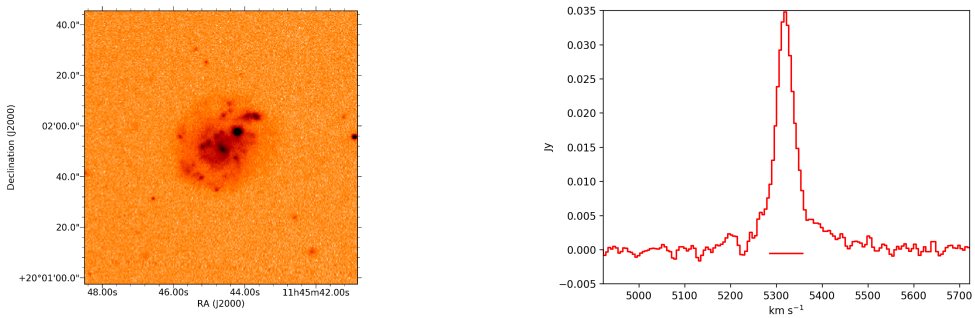

Figure 1.6: Example of the HI profile obtained for a Face-on galaxy (CGCG 97-138) with optical inclination=36.3 degrees. This galaxy doesn't belong to our sample

1.4 Ram Pressure Stripping

When a gas rich late-type galaxy travels through a cluster's intra-cluster medium (ICM) the hot gas in the ICM creates a pressure force against the colder interstellar medium (ISM) disk in the galaxy, and is able to strip some of the galaxy's ISM from it, Gunn Gott(1972). This process is known as ram pressure stripping. During the ram pressure stripping, the old stellar disk is not disturbed but the HI gas is. The principal difference

between the ram pressure stripping and tidal interactions is that tidal interactions impacts both the stellar and gas disks

When the galaxy passes through the ICM, it feels ram pressure that depends on the ICM density and the velocity of the galaxy relative to the ICM Gunn Gott(1972). Given by

$$p_{ram} = \rho \times v_{rel}^2 \tag{1.2}$$

Where ρ is the ICM density and v_{rel} the velocity of the galaxy relative to the ICM. Ram pressure is able to strip the gas from the galaxy when the v_{rel} is high and when the ICM density inside the cluster is sufficiently high. The intracluster medium is not distributed homogeneously, with a higher concentration in the cluster center. It occupies the space between cluster galaxies and when the density is sufficient generates X-ray emissions, produced by thermal bremsstrahlung. The X-ray luminosity is higher in the ICM of rich clusters. The ICM has an electron densities n_e between $10^{-4} cm^{-3}$ and $10^{-2} cm^{-3}$ with a temperature between T $\approx$ 2 $\times 10^7$ K and 2 $\times 10^8 K$. Jachym et al.(2019) reveals a case of ram pressure stripping in ESO 137-001 where a galaxy clearly shows a very widespread tail of stripped gas for the Norma jellyfish galaxy. ESO 137-001 is projected with a few hundred kpc of the core of the ICM rich Norma cluster In figure 1.7, we can clearly see gas in various phases that was ram-pressure stripped forming a one-sided tail.

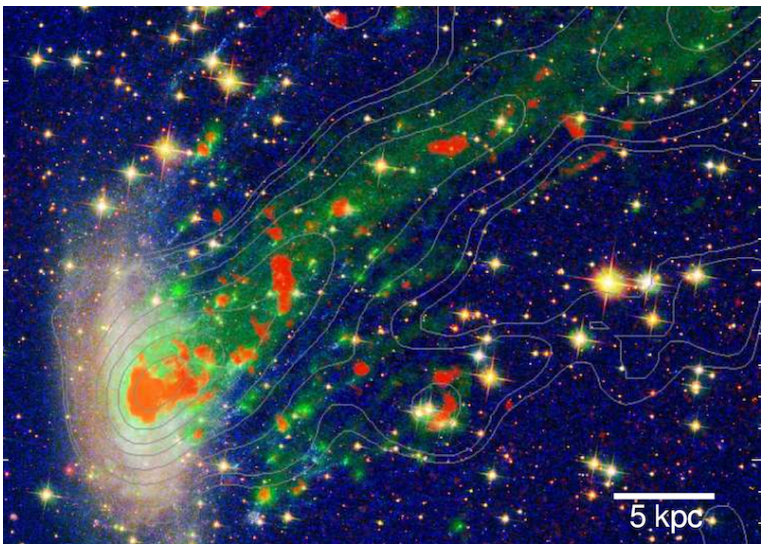

Figure 1.7: Jellyfish galaxy. Plot obtained from Jachym et al.(2019). We can the gas stripped from ESO 137-001 galaxy due to the ram pressure. Orange = CO(2-1), green $H\alpha$ and the contours= X-ray emission.

Ram pressure stripping cannot remove stars from a galaxy but can strip its gas. The effect of ram pressure is particularly strong on HI at the edges of the HI disks because of the weak gravitational forces binding the gas to the galaxy there.

Tidal forces, can strip stars from a galaxy, but ram pressure can have a very strong effect on the galaxy gas while not having enough force to strip stars from the galaxy. Because of this difference, we can identify what kind of interaction a galaxy is undergoing during and for a short period($0.7Gy$) after the interaction. The tidal and ram pressure forces on a galaxy can be strong enough to enhance starformation for at least a short period of time during and right after the interaction Kapferer et al.(2009).

Every type of galaxy is expected to have a certain amount of HI gas because different structures imply different quantities of HI gas with the HI/M^* ratio increasing from early to late type galaxies. When a galaxy has been subject to ram pressure, its HI gas may be stripped from the galaxy, causing an HI deficiency. Comparing the difference between the actual HI gas and the expected HI gas we get the HI deficiency, see section 3.1 for details of how this is calculated.

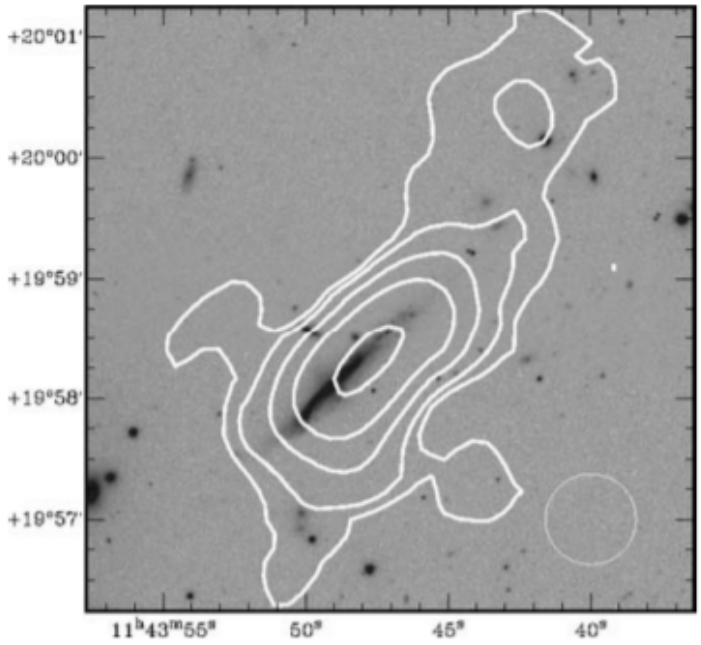

Figure 1.8: Image from CGCG 097-087. The white lines are from the HI surface density map overlayed on a SDSS i-band image. The small circle in the bottom right corner corresponds to the size of the VLA D-array beam. This plot was obtained from Scott et al.(2010).

Ram pressure stripping can have dramatic effects on galaxy evolution. As we approach

the cluster's center, more ISM gas is typically stripped decreasing the star formation. In some cases, the gas can be briefly compressed and temporarily enhance the star formation during ram pressure stripping Kapferer et al.(2009), before this stage is reached.

1.5 Tidal effects

Besides the gas stripping, there is another mechanism that is able to remove matter from the galaxies which is tidal interactions between galaxies. Tidal forces are very complex phenomena, and in clusters these can take two forms. The cluster potential drives infalling galaxies to the cluster core where, due to the higher galaxy density, repeated fast low impact gravitational interactions between galaxies are likely to happen, this process is known as "harassment". Additionally for members of groups entering the cluster slow high impact interactions can also occur. High impact interactions are capable of disturbing and displacing the bulk of the HI in a galaxy. See figure 1.9 from Sengupta et al.(2013)

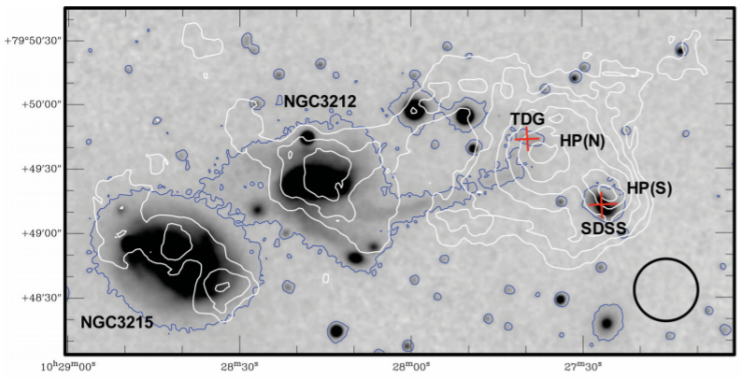

Figure 1.9: Image from Sengupta et al.(2013). HI column density contours in white are overlaid on SDSS g-band image of Arp 181 system. The objects marked with a red cross are tidal dwarf galaxies. The blue contours mark the faint limit for the g-band image and show a tidal tail.

Chapter 2

Sample selection

Our sample consists of 30 galaxies that belong to the Abell 262 cluster within a velocity range of $v_{cluster} \pm 2\sigma$ according to Hassan et al.(2016), which corresponds to $4428 to 5276 kms^{-1}$ and within the 2 $\times$ virial radius of the cluster (70 arcminutes), from Hassan et al.(2016) and most of them with HI spectra available in NED. There are 23 galaxies from this selection but to increase our understanding of environmental effects beyond this radius, we included 7 galaxies outside two times the virial radius with HI spectra. The sample galaxies and their properties are set out on in tables 2.1, 2.2, 2.4 and 2.6

The galaxies CGCG522-036 and CGCG522-047 don't have HI spectra available but were added to our sample because upper limit flux densities are cataloged in Wegner et al. (1993). The hubble types for the galaxies from NED are given in 2.2 and the table shows the sample is dominated by late type galaxies. Galaxies CGCG522-004 and CGCG522-071 have HI spectra but with a signal to noise too low for reliable measurements. For these galaxies we use the data provided by the original authors Springob et al.(2005). The HI spectras were obtained from Arecibo observatory and retrieved from the NED archive. Arecibo is a spherical reflector with 305 meters diameter that consists of perforated aluminum panels that receive the radio waves from a movable secondary reflector located 168 meters above the main dish; this structure can move a few degrees in drift scanning mode.

Table 2.1: Table with galaxies parameters obtained from NED database and parameters calculated with the HI spectra from each galaxy

(1) Galaxy ID	(2) V_{HI} kms^{-1}	(3) w_{20} kms^{-1}	(4) w_{50} kms^{-1}	(5) S/N_{HI}	(6) A_{flux}	(7) $V_{optical}$ kms^{-1}	(8) Distance to center kpc
CGCG 522-001	4496 ± 1	289 ± 1	280	11.8	1.04 ± 0.04	4498	1620
CGCG 522-004	4964 ± 9	723	225	2.4	1.11 ± 0.03	4674	1542
CGCG 522-005	4742 ± 13	80 ± 27	80	3.7	1.16 ± 0.22	4847	1310
CGCG 522-006	5576 ± 1	104 ± 2	96	11.1	1.27 ± 0.08	5559	1864
CGCG 522-007	4739 ± 6	221 ± 12	187	5.5	1.15 ± 0.07	4660	1205
CGCG 522-014	4381 ± 9	491 ± 17	52	2.9	1.15 ± 0.04	4146	1190
CGCG 522-018	5516 ± 8	174 ± 16	130	5.3	1.11 ± 0.17	5499	1114
CGCG 522-020	4147 ± 2	347 ± 4	330	8.1	1.05 ± 0.1	4150	1174
CGCG 522-024	5304 ± 8	256 ± 17	256	4.3	1.13 ± 0.02	5311	336
CGCG 522-025	6056 ± 8	120 ± 17	120	3.7	1.22 ± 0.04	6056	182
CGCG 522-036	-	-	-	-	-	-	23
CGCG 522-038	5534 ± 2	137 ± 5	120	5.1	1.13 ± 0.1	5542	572
CGCG 522-041	6112 ± 23	218 ± 32	96	5.4	1.04 ± 0.13	6131	0
CGCG 522-042	5012 ± 8	296 ± 17	234	7.5	1.23 ± 0.17	5020	444
CGCG 522-046	5425 ± 6	482 ± 12	458	4.2	1.21 ± 0.09	5254	993
CGCG 522-047	-	-	-	-	-	-	196
CGCG 522-050	5746 ± 7	240 ± 14	206	5.1	1.03 ± 0.09	5743	596
CGCG 522-060	4635 ± 5	239 ± 10	239	4.5	1.09 ± 0.02	4617	1044
CGCG 522-062	5633 ± 6	200 ± 13	174	4.1	1.04 ± 0.1	5621	1089
CGCG 522-063	4550 ± 4	204 ± 8	178	6.3	1.15 ± 0.07	4540	606
CGCG 522-064	5531 ± 1	9 ± 1	0	15	1.12 ± 0.7	5359	1216
CGCG 522-069	5213 ± 8	154 ± 17	154	4.4	1.0 ± 0.02	5216	1428
CGCG 522-071	5363 ± 6	906	34	3	1.21 ± 0.11	5336	816
CGCG 522-073	4475 ± 4	212 ± 8	187	5.1	1.17 ± 0.08	4473	1573
CGCG 522-074	4971 ± 2	264 ± 5	256	10.5	1.19 ± 0.07	4967	1813
CGCG 522-086	4900 ± 2	332 ± 3	307	15.5	1.05 ± 0.15	4903	1249
CGCG 522-094	4805 ± 15	332 ± 30	264	8.6	1.06 ± 0.9	4838	1638
KUG 0149+353	4962 ± 6	202 ± 11	176	4.7	1.07 ± 0.04	4959	654
KUG 0151+352	5005 ± 4	149 ± 7	128	5.2	1.33 ± 0.04	5004	830
UGC 01366	5104 ± 8	426 ± 17	426	8.7	1.07 ± 0.02	5113	698

(2) Velocity of the HI gas of the galaxy, obtained from the HI spectra that was retrieved from NED database
(3) 21cm line width at 20% height of the fitted velocity channel with highest HI flux density
(4) 21cm line width at 50% height of the fitted velocity channel with highest HI flux density
(5) Signal-to-noise ratio of the HI spectrum
(6) HI asymmetry parameter
(7) Optical systemic radial velocity, retrieved from NED
(8) Projected distance to the cluster center

Table 2.2: Table with the different parameters used to calculate HI deficiency, HI mass and the star formation rate of the galaxies on our sample

(1) Galaxy ID	(2) redshift	(3) Hubble type	(4) HI Flux Jy km^{-1} s	(5) HI Deficiency dex	(6) C1	(7) C2	(8) FUV Flux Jy (10^{-4})
CGCG 522-001	0.015	Sb	8.15	-0.199	7.82	1.25	12.8 ± 0.33
CGCG 522-004	0.01559	SAb	2.75	0.406	7.75	1.19	-
CGCG 522-005	0.016168	Sa	0.49	0.499	7.75	1.19	0.23
CGCG 522-006	0.01854	Sc	4.94	-0.399	7.16	1.74	-
CGCG 522-007	0.015544	Sab	2.6	-0.171	7.75	1.19	-
CGCG 522-014	0.01383	S0-a	3.63	-0.041	7.75	1.19	0.67 ± 0.12
CGCG 522-018	0.01834	I	3.72	-0.196	7.16	1.74	4.25 ± 0.24
CGCG 522-020	0.01385	Sb	12.91	-0.221	7.82	1.25	1.20 ± 0.41
CGCG 522-024	0.01772	Sbc	1.64	0.102	7.84	1.22	5.03 ± 0.26
CGCG 522-025	0.0202	SABb	0.35	0.655	7.82	1.25	-
CGCG 522-036	0.015057	S0-a	0.95*	0.361	7.75	1.19	-
CGCG 522-038	0.01849	SABc	6.55	-0.304	7.84	1.22	-
CGCG 522-041	0.02045	Sc	2.42	0.189	7.16	1.74	-
CGCG 522-042	0.01674	Sb	0.53	0.95	7.82	1.25	0.13 ± 0.04
CGCG 522-046	0.017525	E-S0	6.4	-0.468	7.75	1.19	0.35 ± 0.09
CGCG 522-047	0.014737	S0-a	1.1*	0.413	7.75	1.19	0.34 ± 0.08
CGCG 522-050	0.01916	Sc	2	0.145	7.16	1.74	-
CGCG 522-060	0.015401	S0-a	0.57	0.015	7.75	1.19	-
CGCG 522-062	0.01875	Sb	1.98	-0.025	7.82	1.25	1.38 ± 0.16
CGCG 522-063	0.01514	SABc	3.22	-0.134	7.84	1.22	3.46 ± 0.06
CGCG 522-064	0.01788	S0-a	1.43	0.563	7.75	1.19	-
CGCG 522-069	0.0174	Sc	1.48	0.342	7.16	1.74	2.74 ± 0.22
CGCG 522-071	0.0178	Sb	0.99	0.89	7.82	1.25	-
CGCG 522-073	0.01492	Sb	2.83	-0.007	7.82	1.25	2.05 ± 0.20
CGCG 522-074	0.01657	Sc	1.71	0.339	7.16	1.74	0.65 ± 0.12
CGCG 522-086	0.01636	SABc	39.99	-0.743	7.84	1.22	-
CGCG 522-094	0.01614	Sab	1.64	0.165	7.75	1.19	-
KUG 0149+353	0.016541	Sb	0.77	0.385	7.82	1.25	0.68 ± 0.09
KUG 0151+352	0.016692	Sb	0.69	0.277	7.82	1.25	1.30 ± 0.09
UGC 01366	0.017055	SBc	0.89	0.825	7.16	1.74	0.52 ± 0.04

(2) Redshift from NED
(3) Morphological Hubble type of the galaxies from NED
(4) HI flux obtained from NED
(5) HI deficiency. The values with * are upper limits
(6) Constant C1 for galaxy Hubble type (Solanes et al. (2001))
(7) Constant C2 for galaxy Hubble type (Solanes et al. (2001))

Table 2.3: Table with all galaxy parameters obtained

Table 2.4: Table Title

(1) Galaxy ID	(2) Ks	(3) K flux density $erg\ cm^{-2}\ Hz^{-1}\ (10^{-25})$	(4) K luminosity density $ergHz^{-1}(10^{29})$	(5) SFR $M_{\odot}yr^{-1}$	(6) Stellar mass $M_{\odot}(10^9)$	(7) HI mass $M_{\odot}(10^9)$
CGCG 522-001	-	-	-	1.79	-	9.42
CGCG 522-004	-	-	-	-	-	3.18
CGCG 522-005	-	-	-	0.03	-	0.567
CGCG 522-006	-	-	-	-	-	5.71
CGCG 522-007	-	-	-	-	-	3.0
CGCG 522-014	9.9	7.31	4.127	0.094	8.79	4.198
CGCG 522-018	-	-	-	0.59	-	4.3
CGCG 522-020	10.25	5.297	2.9899	1.67	6.16	14.93
CGCG 522-024	10.84	3.076	1.736	0.7	3.38	1.896
CGCG 522-025	12.06	1	56.45	-	0.976	0.405
CGCG 522-036	-	-	-	-	-	1.09*
CGCG 522-038	10.09	6.138	3.4647	-	7.25	7.57
CGCG 522-041	10.86	3.02	1.7059	-	3.31	2.798
CGCG 522-042	10.2	5.546	3.1308	0.018	6.48	0.613
CGCG 522-046	10.22	5.445	3.07379	0.049	6.35	0.659
CGCG 522-047	9.61	9.5499	5.3909	0.047	1.27	1.18*
CGCG 522-050	11.94	1.117	0.6305	-	1.1	2.31
CGCG 522-060	12.88	0.4699	26.525	-	0.424	1.099
CGCG 522-062	12.04	1.0186	57.499	0.19	0.996	2.29
CGCG 522-063	12.76	0.5248	29.625	0.48	0.479	3.72
CGCG 522-064	8.89	3.02	1.70	-	2.46	-
CGCG 522-069	10.94	2.805	1.58	0.38	3.05	-
CGCG 522-071	10.57	3.945	2.23	1.14	-	4.45
CGCG 522-073	12.72	0.545	30.7	0.29	0.498	3.27
CGCG 522-074	12.41	0.724	40.89	0.091	0.683	1.98
CGCG 522-086	9.37	11.91	6.7245	-	46.2	15.1
CGCG 522-094	10.1	6.08	3.4329	-	7.17	1.896
KUG 0149+353	12.39	0.7379	41.65	0.094	6.97	0.89
KUG 0151+352	-	-	-	0.18	-	7.4
UGC 01366	10.3	5.0585	2.855	0.073	5.85	1.03

(2) 2MASS Ks magnitude in the AB system, from NED
(3) Ks flux density calculated from (2)
(4) Ks luminosity density calculated from (3)
(5) Star formation rate (from FUV)
(6) Stellar mass in units of $10^9 M_{\odot}$
(7) HI mass in units of $10^9 M_{\odot}$. The values with * are galaxies with upper limits for the HI flux

Table 2.5: Table with all galaxy parameters obtained

Table 2.6: Table Title

(1) Galaxy ID	(2) B-I mag	(3) inclination degrees	(4) V_{rot} kms^{-1}	(5) R.A. degrees	(6) Declination degrees	(7) d_{pro} arcmin
CGCG 522-001	1.66	50	185	26.594458	36.460306	79.577
CGCG 522-004	2.27	90	351	26.817292	35.563306	75.719
CGCG 522-005	1.88	58	46	26.875667	36.034917	64.346
CGCG 522-006	-	9	334	26.931833	35.022528	91.576
CGCG 522-007	2.05	62	122	27.029441	36.453242	59.198
CGCG 522-014	2.54	60	276	27.35725	35.452889	58.467
CGCG 522-018	1.1	55	104	27.636585	35.359687	54.733
CGCG 522-020	1.68	55	207	27.684083	35.284528	57.66
CGCG 522-024	1.65	50	164	27.871458	36.065944	16.5
CGCG 522-025	2.01	46	82	28.0115	36.131028	8.975
CGCG 522-036	-	33	-	28.173	36.144	1.154
CGCG 522-038	-	23	123	28.191333	36.619306	28.076
CGCG 522-041	-	46	270	28.22475	36.052889	0
CGCG 522-042	2.06	72	199	28.239417	36.512889	21.796
CGCG 522-046	2.15	83	416	28.345667	36.955139	48.769
CGCG 522-047	2.28	53	-	28.373542	36.221306	9.61
CGCG 522-050	1.33	55	123	28.472509	36.585084	29.273
CGCG 522-060	2.08	29	172	28.74475	35.422806	51.254
CGCG 522-062	2.43	24	122	28.757833	36.919917	53.502
CGCG 522-063	1.37	90	122	28.795	36.260722	29.78
CGCG 522-064	-	59	9	28.792542	35.281889	59.741
CGCG 522-069	-	90	184	28.993667	37.129389	70.155
CGCG 522-071	-	42	438	29.021958	36.129083	40.092
CGCG 522-073	1.64	47	121	29.099208	37.215861	77.278
CGCG 522-074	1.15	62	127	29.087875	37.452194	89.058
CGCG 522-086	1.81	34	244	29.425833	35.916111	61.366
CGCG 522-094	1.94	42	219	29.728625	36.674694	80.432
KUG 0149+353	2.37	49	104	28.002	35.639083	32.138
KUG 0151+352	7.4	-	81	28.546616	35.5348	40.757
UGC 01366	2.14	79	209	28.5825	36.629806	34.267

(2) B-I color index
(3) Inclination, determined from optical data, in degrees
(4) Rotational velocity of the HI gas
(5) Right Ascension (J2000), retrieved from NED
(6) Declination (J2000), retrieved from NED
(7) Projected distance to the cluster center

Chapter 3

Methodology

3.1 HI deficiency

The HI deficiency of a galaxy is obtained by comparing the expected HI mass of a galaxy with the actual HI mass present. Several links exist between the gas deficiency and the characteristics of the galaxies, such as their Hubble type and optical diameter. Figure 3.1 the top panel shows the fraction of galaxies with HI deficiencies > 0.3 from 1900 galaxies in a sample of 18 galaxy clusters from Solanes et al. (2001). In the bottom of the figure shows the measured HI deficiency with respect to their clustercentric radius. In figure 3.2 we can see the HI deficiency increase with of the Coma and A1367 clusters. We also see that there is a natural variation in HI deficiency outside the clusters of +/- 0.3 dex.

The NASA/IPAC Extragalactic Database(NED) is a database of extragalactic objects and their properties in which astronomical objects information cross-correlates such as names, positions, redshifts, and basic data. With the Arecibo HI spectra obtained from NED (Springob et al.(2005)). We are able to measure the galaxies V_{HI}, A_{flux}, w_{20}, and the signal-to-noise. Using Haynes et al.(1984) equations, we are able to calculate the expected mass of HI present in our sample galaxies and the expected HI mass. The expected HI mass is dependant on the Hubble type of the galaxy with the constants C1 and C2 are related to the galaxy's Hubble type from Solanes et al. (2001) and it's optical diameter, D (kiloparsecs).

$$\log(M_{HIexpected}(M_{\odot})) = C1 + C2\log(D) \tag{3.1}$$

To calculate the actual HI mass present in a galaxy we use distance to the cluster (C_d) in units of Mpc and the integrated HI flux density (Sdv) in units of Jy km s^{-1},

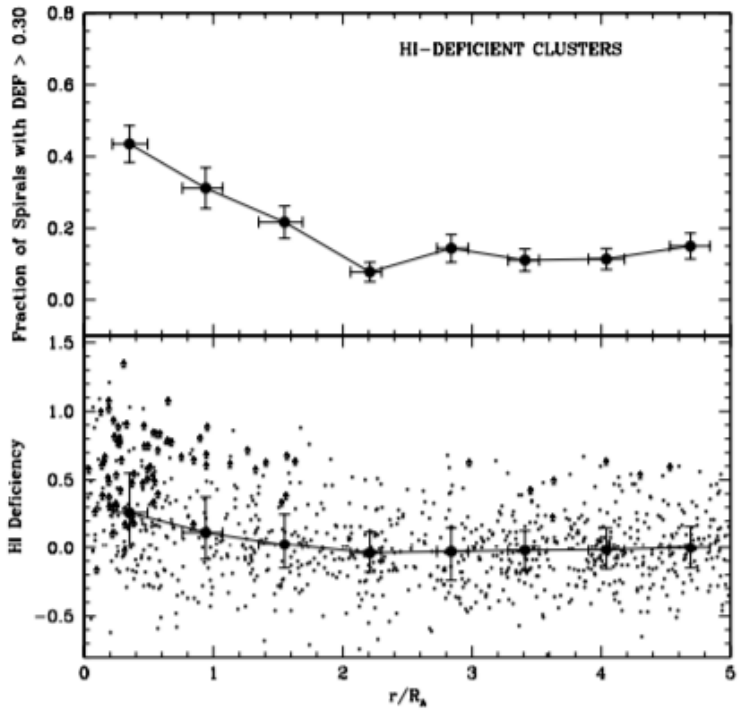

Figure 3.1: In this plot from Solanes et al. (2001) we can see how the fraction of galaxies with HI deficiency is enhanced when approaching the cluster center.

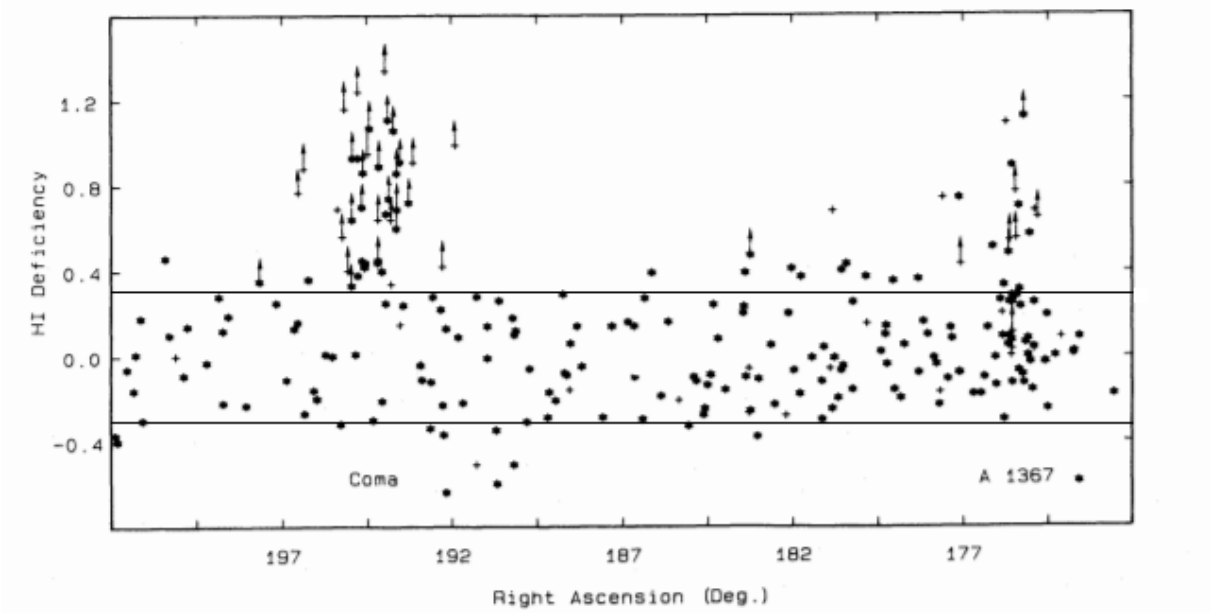

Figure 3.2: Modified figure from Gavazzi et al.(1989) showing the HI deficiency of 252 galaxies that belong to the Coma and A1367 clusters against the right ascension. Lower limits are marked with arrows, S0a galaxies are marked with plus signs, and later galaxy types than Sa are marked with an asterisk. The black horizontal lines at 0.3 and -0.3 indicate the values of HI deficiency at which it's likely that the galaxies in fact have a HI deficiency or excess.

$$M_{HIpresent}(M_{\odot}) = 2.36 \times 10^5 C_d^2 \int Sdv \tag{3.2}$$

This way we get the actual HI mass and the theoretical HI mass for a galaxy and calculate its HI deficiency using equation 3.3. A galaxy with a higher content of HI than expected is a galaxy with a negative HI deficiency. In the case of a galaxy with a positive HI deficiency, above the 0.3 dex threshold, we can determine that this galaxy was likely stripped of its HI content.

$$HI_{def} = \log(M_{HIexpected}) - \log(M_{HIpresent}) \tag{3.3}$$

3.1.1 A_{flux}

A_{flux} is the asymmetry of a galaxy's integrated HI flux density profile at velocities above and below the galaxy systemic velocity. The systemic velocity is the mean of the upper and lower W_{20} velocity limits. The A_{flux} is a useful parameter to determine recent or ongoing disturbances to a galaxy's HI disk. The HI disk was likely recently disturbed or is still being stripped if the $A_{flux} > 1.26$. Where 1.26 is the 2σ of the distribution of A_{flux} from a sample of isolated galaxies Espada et al.(2011).

In figure 3.3 we can see a galaxy with a very low A_{flux} and its HI profile not disturbed. While on figure 3.4 we have a galaxy with a very high A_{flux} and a asymmetrical HI profile.

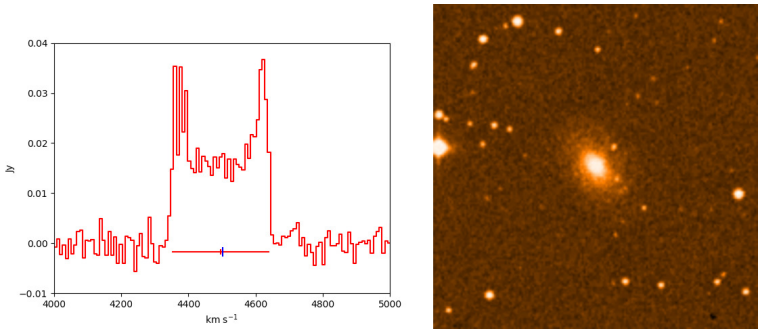

Figure 3.3: Galaxy CGCG522-064. This galaxy has a A_{flux}=1.04

The A_{flux} was calculated using a python program developed by T. Scott. In this program we calculate the A_{flux} using the HI profile of the galaxies and also calculate the V_{HI} and W_{20}.

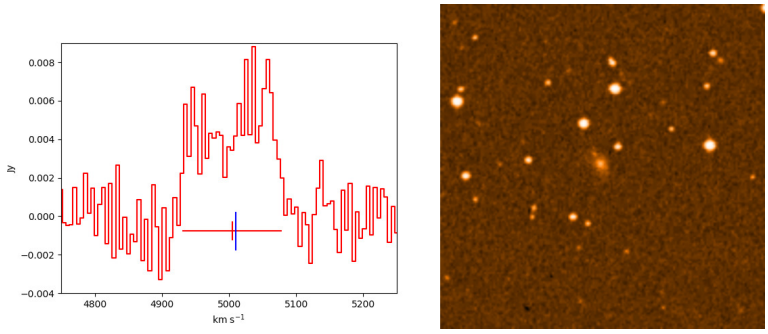

Figure 3.4: Galaxy KUG 0151+352. This galaxy has a A_{flux}=1.33

3.1.2 HI rotation velocity

The inclination(I) of the galaxies was derived using the equation,

$$\sin(i) = \sqrt{\frac{1-(\frac{b}{a})^2}{1-q_0^2}} \tag{3.4}$$

Being a and b the major and minor axes and q_0 the intrinsic axial ratio for which we use 0.3 And for the rotation velocity of the galaxies,

$$v_{rot} = \frac{1}{2}\frac{w_{20}}{\sin(i)} \tag{3.5}$$

Where W_{20} is the line-width at 20% of the flux density in the channel with highest HI flux density. Ideally we would use the HI major and minor axes in these calculations but in our case we do not have these values so we use the optical axes instead when applying equation 3.4.

3.2 Galaxies Stellar mass

The Two Micron All-Sky Survey(2MASS) was a survey of the entire sky scanning in three near-infrared bands, creating a massive astronomical catalog. This survey contains the K magnitude for several galaxies of our sample galaxies. The K-band was obtained from hyperleda* database retrieving the 14 × 14 arcsec aperture flux and then converted the magnitude to the AB system using equation 3.6 from Skrutskie et al. 2006)

$$m_{AB} = m_{vega} + 1.84 \tag{3.6}$$

*http://leda.univ-lyon1.fr/

Having the magnitude in the AB system we can calculate the flux density F with the general formula (see eg Willmer 2018),

$$m_{AB} = -2.5 \log F - 48.6 \tag{3.7}$$

With the luminosity distance $d_L = 69 Mpc$ from NED, assuming $H_0 = 73 km/sec/Mpc$, $\Omega_{matter} = 0.27$, $\Omega_{vacuum} = 0.73$, and the flux density using equation 3.7 we can calculate the Luminosity density, L, $(ergs^{-1}Hz^{-1})$ using equation 3.8

$$L = 4\pi d_L^2 F \tag{3.8}$$

With the luminosity density and the equation 3.9, from Wen et al.(2013) we can calculate the galaxies stellar mass. We have a luminosity density but need the actual luminosity, which we get by multiplying the luminosity density by ν. The ν is the interval of frequencies, $\nu_{min} = 1.27 \times 10^{14} Hz$ up to $\nu_{max} = 1.53 \times 10^{14} Hz$, which gives us ν=2610.4 $\times 10^{10} Hz$. Being $L_\odot$ the solar luminosity $L_\odot = 3.826 \times 10^{33}$ erg s^{-1},$M_\odot$ the solar mass we can calculate the galaxies stellar mass, using equation 3.9

$$log(M/M_\odot) = -0.498 + 1.105 log(\upsilon L/L_\odot) \tag{3.9}$$

3.3 Star formation Rate

Star formation indicators such as the far-ultraviolet (FUV) fluxes can be used to get a good estimate of the star formation rate. We chose to use the elliptical Kron aperture flux measurements, obtained with GALEX and available in NED. In such a measurement, the first image moment is used to determine the elliptical aperture from which the flux of the galaxy is integrated, according to what was proposed by Kron R.G. (1980). But we still need to take into account the obscuration that the interstellar dust has on the flux that arrives at the telescope. To calculate the flux density F using equation 3.10, we multiply f, the flux directly extracted from NED, by a factor of 1.765 to correct for the galactic extinction in the direction of the cluster. The factor 1.765 was obtained using the Cardelli et al.(1989) extinction law at the effective wavelength of the FUV (1528 Angstroms) and the Schlafly & Finkbeiner(2011) extinction maps at the A262 position where we only used 1 single value for the whole region since their maps have a resolution of 2 degrees.

$$F = 1.765f \tag{3.10}$$

Then calculate the Luminosity density using equation 3.8

With the luminosity density, we are able to calculate the star-formation rate, SFR(UV), using the equation 3.11, from Lee et al.(2009)

$$SFR(UV) = 1.4 \times 10^{-28} L \tag{3.11}$$

SFR(UV) is in solar masses per year($M_\odot\ yr^{-1}$)

To reflect the ongoing star formation relatively to the galaxy's mass we explore the specific star-formation rate, sSFR(yr^{-1}), defined as the SFR per unit of stellar mass.

$$sSFR = \frac{SFR(UV)}{M} \tag{3.12}$$

Being SFR(UV) the star formation rate calculated with equation 3.11 and M the galaxy's stellar mass in units of $M_\odot$

3.4 Statistics

Pearson's correlation coefficient also known as the r-value is the statistical test used to measure the statistical association between two variables. It ranges between -1 and 1, where a value of 1 indicates that two variables are linearly related. A value of -1 indicates that the data is negatively linearly related and a value of 0 indicates that the variables have no linear relation.

The p-value shows the statistical significance of the data and ranges between 0 and 1. It evaluates the probability of our data rejecting the null hypothesis. The null hypothesis states that there is no relation between our data. As we get a smaller p-value the stronger evidence that there is a relationship between the two variables in the study. Getting a p-value inferior to 0.05 indicates strong evidence that the variables are related with a less than 5 % probability that the variables are not related. This value doesn't tell us that there is a 95 percent probability that our hypothesis is true, only states that the hypothesis of no relationship between two variables should be ignored.

The critical values of the Pearson product-moment correlation coefficient is the point with which we compare to the r-value obtained from our sample to determine if we reject the null hypothesis or not. If the absolute value from our test is greater than the critical

value we assume there is a statistical significance and reject the null hypothesis, that is the two variables are not linearly correlated.

Chapter 4

Results

In this section, our results are discussed after having applied the methods from Chapter 3 to the HI detected A262 sample galaxies from Chapter 2 and analyzing the most important correlations and possible trends within our sample. In the first part, we discuss the properties of the sample as a whole and how the A_{flux}, HI deficiency, HI and stellar mass, and SFR are related in Abell262. Then, we look at selected galaxies individually by analyzing their HI content, HI and stellar mass, and SFR to search for signals of tidal effects and ram pressure stripping.

4.1 Global trends within the cluster

4.1.1 HI deficiency

First, we look at the HI deficiency of the galaxies, which is an indicator of the degree to which the galaxies have partially lost their HI. In cases where HI observations have been made but no HI was detected, then we assume that the HI gas has most likely already been stripped or for lower mass galaxies the HI mass is below the detection threshold and we have upper limits for 2 of these HI non-detections.

We anticipated that the fraction of galaxies with HI deficiencies > 0.3 should increase as we approach the center of the cluster due to the ICM density increase since ram pressure stripping can more easily remove the HI gas from the galaxies that transit in the cluster's center. Also, we would expect galaxy harassment to be more effective near the cluster centre because of the higher density of galaxies there. Figure 4.1, shows the plot of the HI deficiency against the distance to the cluster center for the 30 galaxies in our sample. The Pearson r correlation coefficient from the table 4.1 indicates a moderate but statistically

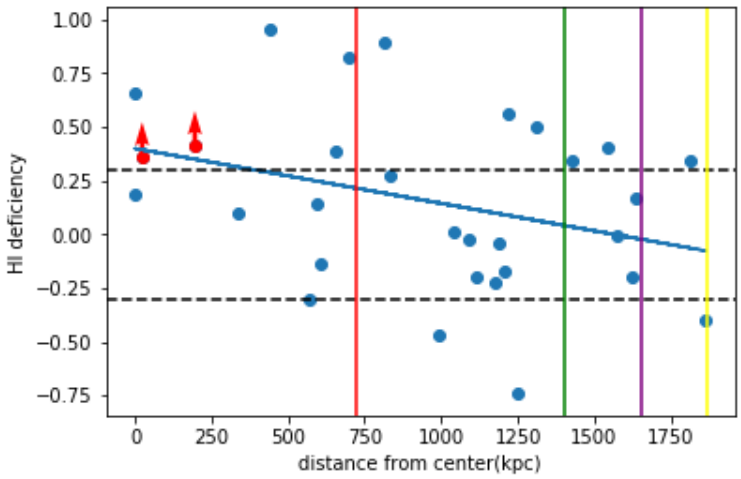

Figure 4.1: Relation between the HI deficiency of the galaxies from our sample and their distance to the center of the cluster. The dashed lines at 0.3 and -0.3 indicate the values of HI deficiency above and below which it's likely that the galaxies in fact have a HI deficiency or excess. The Red line marks the virial radius using the velocity dispersion from Hassan et al.(2016) and the green line is 2 times the Hassan virial radius. The purple line is the virial radius calculated using the Fadda et al. (1996) velocity dispersion and the yellow from Neill et al. (2001). The blue line is the linear fit to the data. The Pearson r=-0.32 and p value=0.08.

significant trend for HI deficiency to increase with proximity to the center of the cluster as we expected. In Gavazzi et al.(1989), the Coma cluster shows a stronger increase in HI deficiency towards the center of the cluster. Looking at figure 1.2, we can see that Abell262 is a cluster with very low x-ray luminosity compared to other nearby clusters; in clusters with high x-ray luminosity, like the Coma cluster, this trend is much stronger, most likely because of stronger ram pressure stripping near the cluster center. Figure 4.1 also shows two alternative virial radii derived from the literature.

We compared the A_{flux} to the distance to the center of the cluster for the 28 galaxies in our sample with HI spectra, in figure 4.2. Larger A_{flux} values near the cluster centre would indicate ongoing HI stripping there. But there is no visible trend, which is confirmed by the Pearson r=-0.12 in table 4.1. This suggests that the galaxies in our sample lost their HI longer ago than the HI relaxation time scale of 0.7 Gyr, Holwerda et al.(2011). The two galaxies with $A_{flux} > 1.26$, CGCG 522-006 and KUG 151+352, are at cluster centric distances 1864 kpc and 830 kpc from the cluster center respectively, suggesting these may be impacted by tidal forces rather than ram pressure interactions. Given A262's low X-ray luminosity detectable ram pressure stripping signature are expected only with a few hundred kpc of the cluster core. When the A_{flux} is > 1.26 it indicates the boundary in which

we can consider the HI disk of the galaxy to be disturbed by environmental effects. The A_{flux}=1.26 line in the plot is the 2 σ value from the AMIGA sample of isolated galaxies, Espada et al.(2011).

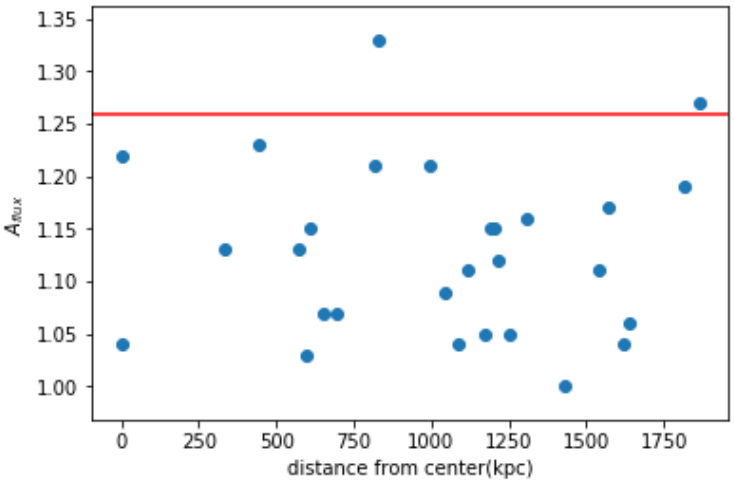

Figure 4.2: A_{flux} of the galaxies against the distance to the center of the cluster. The line at A_{flux}= 1.26 represents the value above which the HI profile asymmetry is likely reflecting an ongoing tidal or ram pressure interaction.

To get a better view of the relation between the HI deficiency and the A_{flux}, we plotted these two measurements to analyze any possible relation between them. No correlation is found between them, Pearson r=0.11 per Table 4.1. In figure 4.3, if we consider that the galaxies with a high A_{flux} are likely currently being stripped of their gas, as the HI stripping progresses they will gain an HI deficiency and their HI disk will eventually return to equilibrium again, in this future situation they may display a lower A_{flux} and high HI deficiency. This is a possible explanation for the galaxies with high HI deficiency but without a high A_{flux}.

Watts et al. (1993) suggested that the A_{flux} values increase at a lower signal to noise. Figure 4.4 shows some galaxies with a very low signal-to-noise ratio but there isn't any trend with A_{flux}, as confirmed by the Pearson value r=-0.05 per Table 4.1.

We hypothesise interactions perturbing the HI measured by A_{flux} >1.26 might be triggering star formation so we looked for a correlation between the A_{flux} and the B-I color, since bluer galaxies tend to be actively forming new stars. However we observe no correlation between this color and the A_{flux} in figure 4.5, Pearson r=0.00 per Table 4.1. The B band we use only considers a correction for the mean atmospheric extinction and the I band doesn't have any correction. This lack of correction may cause an incorrect value

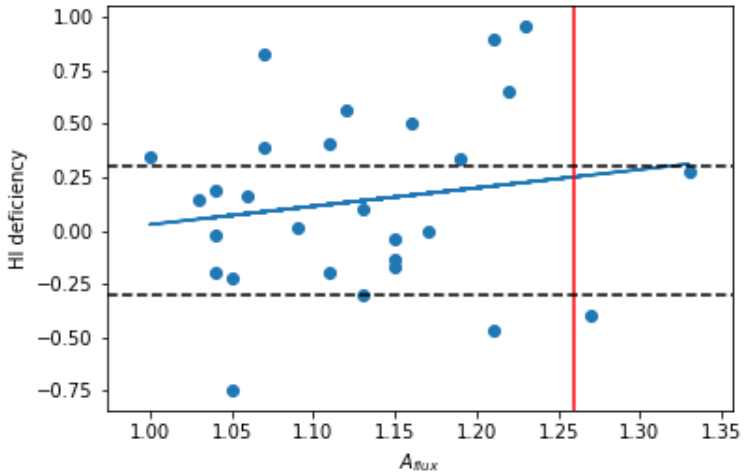

Figure 4.3: Relation between HI deficiency and the A_{flux}. The dashed lines at 0.3 and -0.3 indicate the values of HI deficiency above and below which it's likely that the galaxies in fact have a HI deficiency or excess. The vertical line at 1.26 represents the value above which the A_{flux} indicates that the galaxies are likely to be suffering interactions which are disturbing their HI content. The blue line is the linear regression of the data.

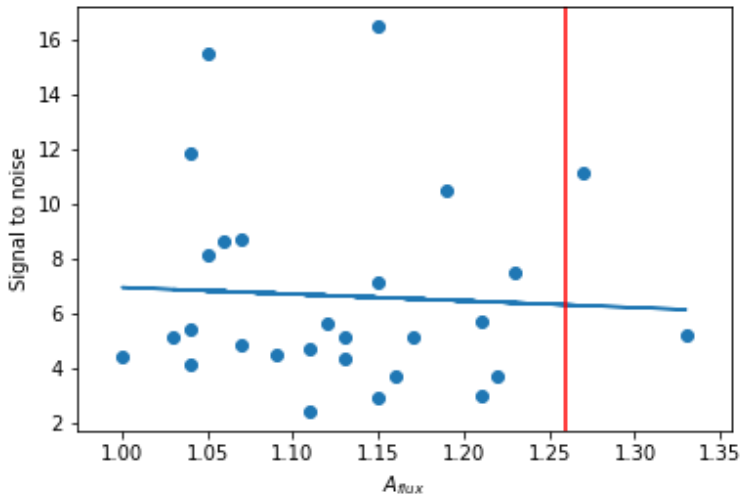

Figure 4.4: Signal to noise ratio against the A_{flux} for our sample galaxies from the HI spectra. The line at 1.26 represents the value at which the HI profile asymmetry (A_{flux}) is likely reflecting a tidal or ram pressure interaction. The blue line is the linear regression of the data.

for both B and I bands. Also the galaxies with a A_{flux} >1.26 don't have available B or I magnitudes, so we cannot come to a firm conclusion based on this plot.

The V_{rot} is expected to increase with the total mass (baryonic+dark matter). As seen in 4.6 there is a trend for HI deficiency to decrease with the increase V_{rot} with a r=-0.32 which is higher than the corresponding critical value. This implies at a level of significance

of 0.1, that a negative correlation between these two parameters. This is an expected relation as we would expect higher mass galaxies to be more resistant to gas stripping. Figure 4.7 shows there is no clear trend between A_{flux} and V_{rot}, which is confirmed by the r value=0.14. This shows that there is no relation between these two parameters.

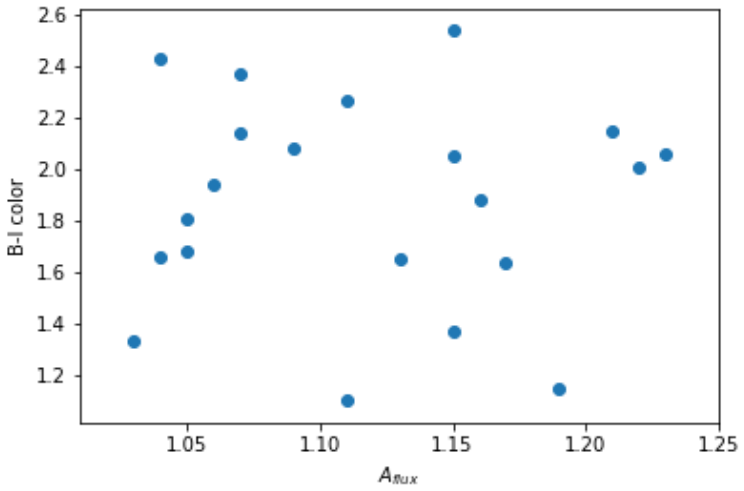

Figure 4.5: B-I color against the A_{flux} for our sample galaxies with B and I photometry.

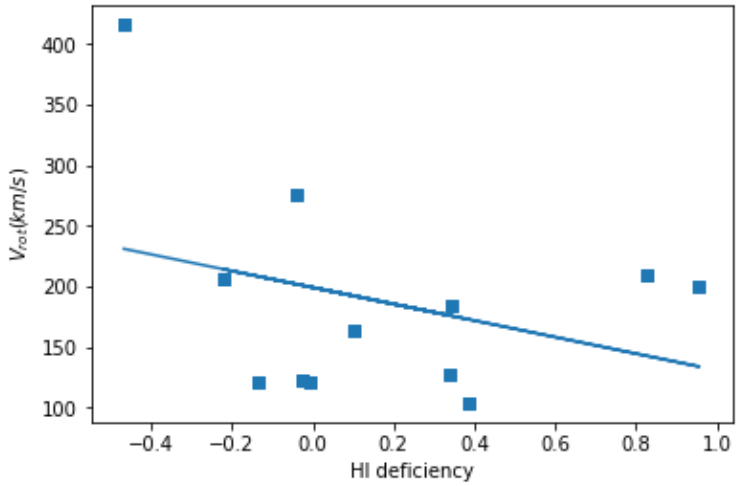

Figure 4.6: HI deficiency vs V_{rot}. The blue line is the linear regression of the data.

The most significant results in this section were the HI deficiency relation with the distance to the cluster center and the relation of the HI deficiency with the V_{rot}. Both with a level of significance of 0.1. Both relations are consistent with expected HI properties in response to the cluster environment.

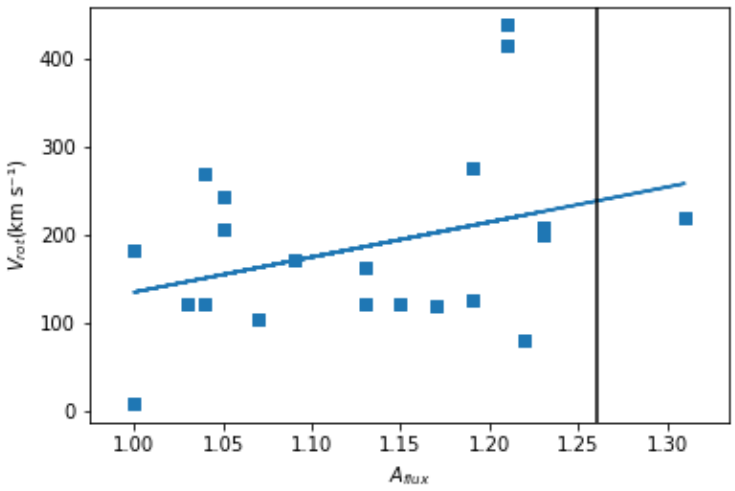

Figure 4.7: Relation between A_{flux} and Vrot. The blue line is the linear regression of the data. The line at 1.26 represents the value at which the HI profile asymmetry (A_{flux}) is likely reflecting a tidal or ram pressure interaction.

Table 4.1: Pearson correlation coefficients r and p, the critical r and level of significance values for the HI deficiency and A_{flux} parameters

Variables	r	p	Number of data points	critical r	level of significance
HI deficiency vs distance	-0.32	0.08	30	0.306	0.1
A_{flux} vs distance	-0.12	0.86	28	0.317	0.1
A_{flux} vs HI deficiency	0.11	0.58	28	0.317	0.1
A_{flux} Signal to noise	-0.05	0.78	28	0.317	0.1
A_{flux} vs color B-I	0.00	0.99	13	0.576	0.1
HI deficiency vs Vrot	-0.32	0.30	28	0.317	0.1
Vrot vs A_{flux}	0.14	0.49	28	0.317	0.1

4.1.2 Galaxies stellar and HI masses

For our sample galaxies, we can consider the relation between the stellar mass and the HI mass. For the majority of the galaxies in our sample baryonic mass is dominated by the stellar mass, as seen in figure 4.8.

The HI deficiency of the galaxies is reflects actual HI gas in a galaxy relative to the HI expected for the galaxy Hubble type and optical size. In figure 4.9 we can see that the galaxies with the highest HI content either have HI excess or don't have an HI deficiency and the galaxies with high HI deficiency are the galaxies with the lowest HI mass from our sample. The HI mass has a clear correlation with the HI deficiency, with a pearson r=-0.61, which corresponds to a level of significance=0.01 per table 4.1. This might indicate more massive galaxies have more HI and are harder to strip of their HI as implied by relation between V_{rot} and HI deficiency in section 4.2. One way to test this is to look at HI deficiency versus stellar mass.

Analysing the correlation of the stellar mass with the HI deficiency, we would expect galaxies with high stellar content to be less affected by environmental effects, since their larger mass should make them less susceptible to these processes. But the data shows no correlation between these two parameters as seen in figure 4.10, with a pearson r=-0.03 per table 4.1. This suggests that the stellar mass of the galaxies doesn't play a major role in determining the HI deficiency of our sample galaxies but the total mass including dark matter does

The relation between the HI deficiency with the total baryonic mass of the galaxies might follow a similar trend. When comparing the HI deficiency with the baryonic mass of the galaxies as seen in figure 4.11, the data points show a similar relation to HI deficiency versus HI mass shown in figure 4.9, but with greater scatter.

The Tully-Fisher relation shows a correlation between the stellar luminosity and the HI v_{rot} for spiral galaxies. This also implies the Tully-Fisher can be expressed as a relation between stellar mass and HI v_{rot}, linked by a mass to light ratio. The V_{rot} parameter in the relation reflects the total (baryonic + dark matter) mass of each galaxies. The relation is tighter for baryonic mass (gas+stars) and v_{rot} than for stars alone and is known as the Baryonic Tully fisher relation(BTFR) McGaugh et al.(2000).

As shown in figure 4.12 there is no clear relation between the HI content of the galaxies with the v_{rot} of the galaxy. While the stellar content, as seen in figure 4.13 shows that there is a clear trend where the increase of the v_{rot} implies an increase of the stellar mass

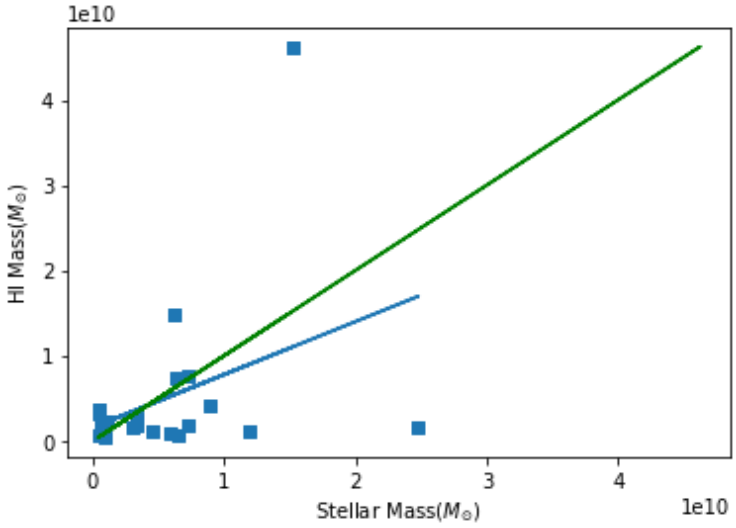

Figure 4.8: Stellar mass compared to the HI mass. The green line is a 1:1 reference. Blue line is the linear regression, which shows a bigger prevalence of the stellar mass in the galaxies of our sample

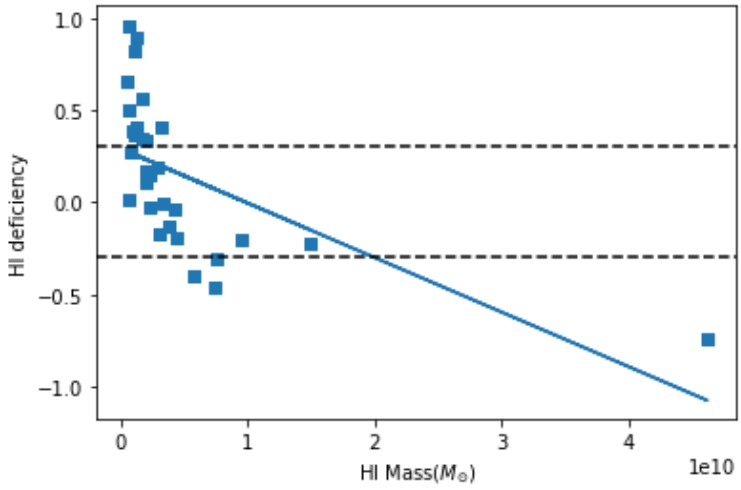

Figure 4.9: HI mass and corresponding HI deficiency for our sample. The dashed lines at 0.3 and -0.3 indicate the values above and below which the galaxies are likely to have an HI deficiency or excess. The blue line is the linear regression of the data.

of the galaxies, with a pearson r=0.48 which corresponds to a level of significance=0.02, per table 4.2. In contrast, the baryonic Tully-Fisher relation (see figure 4.14) has a smaller r=0.34 in table 4.2. This suggests that the cluster environment is causing a departure from the BTFR, while the stellar Tully-Fisher relation remains intact.

We expect A_{flux} to decrease in galaxies with high stellar and HI content because larger mass galaxies are more resilient to environmental effects, unless they are close to the cluster center. For both the stellar and HI mass we see a trend for A_{flux} to increase as mass declines

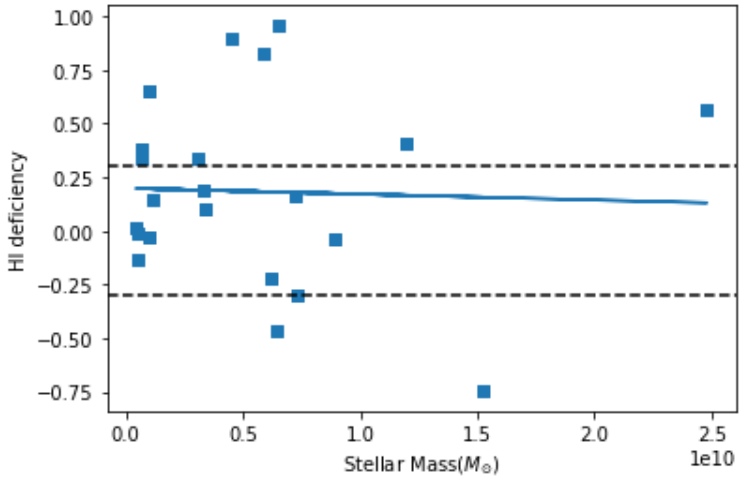

Figure 4.10: Stellar mass and corresponding HI deficiency for our sample. The dashed lines at 0.3 and -0.3 indicate the values above and below which the galaxies are likely to have an HI deficiency or excess. The blue line is the linear regression of the data.

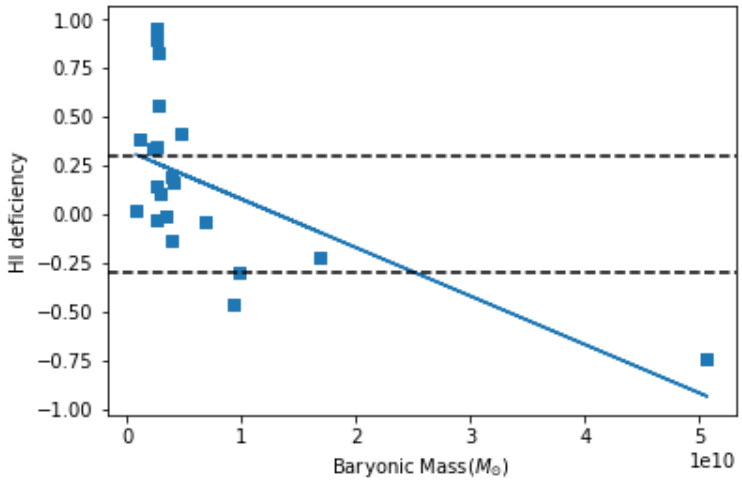

Figure 4.11: Baryonic mass and corresponding HI deficiency. Dashed lines at 0.3 and -0.3 indicate the values above and below which HI deficiency it's likely that the galaxies in fact have a HI deficiency or excess. The blue line is the linear regression of the data.

in both figures 4.15 and 4.16 with pearson r=-0.24 and r=-0.18, respectively, although in neither case is the trend statistically significant. This trend is more clearer with the HI mass because as we seen in figure 4.9 the HI deficiency is correlated with the HI content which is also correlated with the A_{flux}. Galaxies with high baryonic mass tend to have less disturbed HI disks.

In this section the most statistically significant correlations found were between the HI mass and HI deficiency(r =-0.61), Baryonic mass and HI deficiency(r=-0.62) confirming

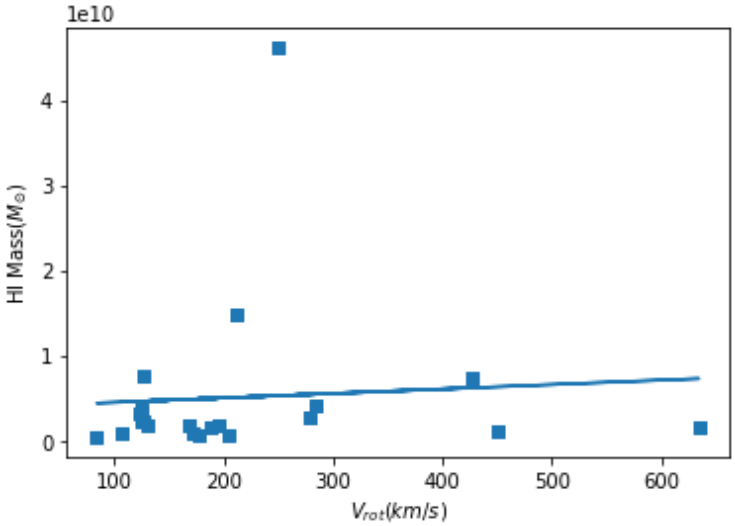

Figure 4.12: HI mass and rotational velocity of our sample. The blue line is the linear regression of the data.

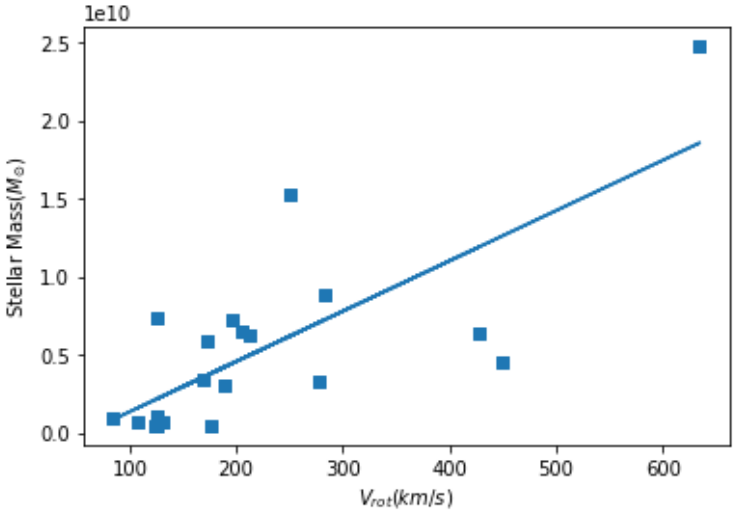

Figure 4.13: Stellar mass and HI rotational velocity of our sample. The blue line is the linear regression of the data.

that galaxies with higher baryonic content are better able to resist HI removal. Statistically significant correlations were also found between stellar mass and V_{rot} (r=0.48) and baryonic mass and V_{rot}(r=0.34). The better correlation with stellar mass compared to baryonic suggests the cluster environment is more heavily impacting the HI compared to the stellar content of its galaxies as expected.

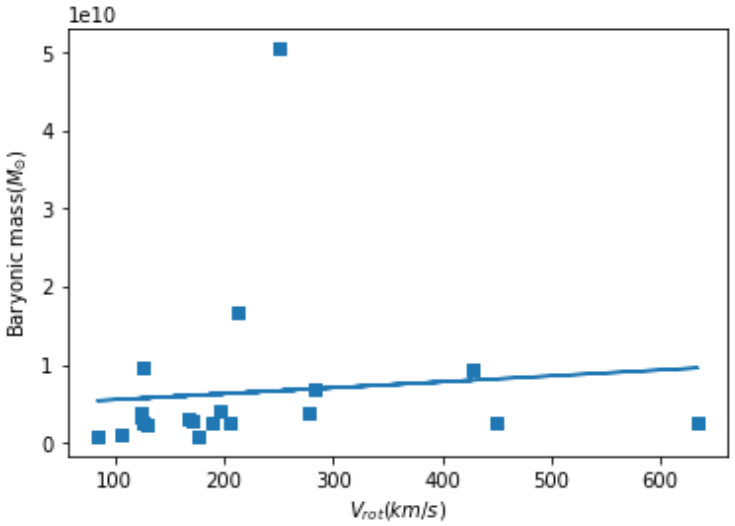

Figure 4.14: Baryonic mass and rotational velocity of our sample. The blue line is the linear regression of the data.

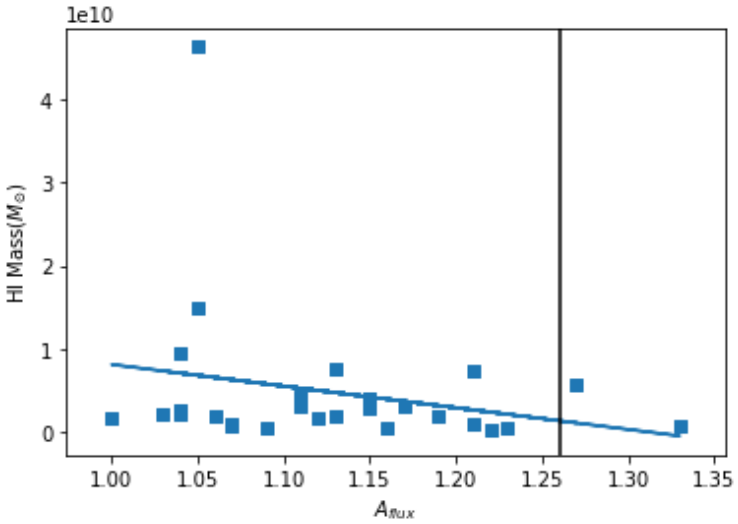

Figure 4.15: Relation between the HI mass of the galaxies with the A_{flux} parameter. The blue line is the linear regression of the data. The line at A_{flux}= 1.26 represents the value above which the HI profile asymmetry is likely reflecting an ongoing tidal or ram pressure interaction.

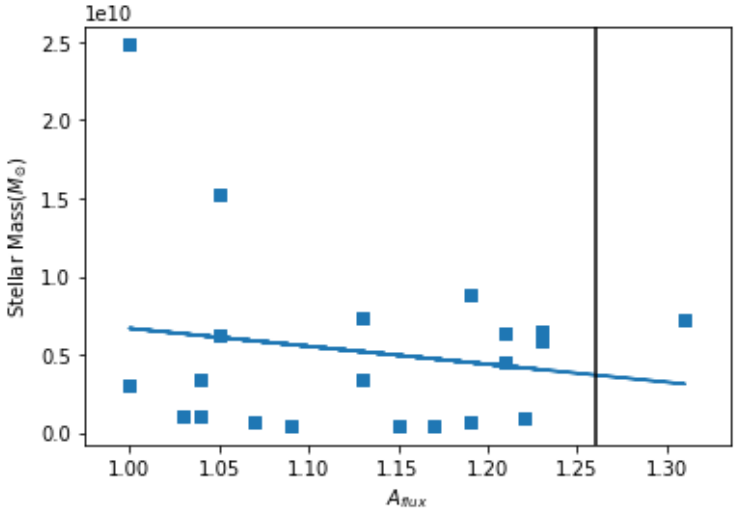

Figure 4.16: Relation between the Stellar mass of the galaxies with the A_{flux} parameter. The blue line is the linear regression of the data. The line at A_{flux}= 1.26 represents the value above which the HI profile asymmetry is likely reflecting an ongoing tidal or ram pressure interaction.

Table 4.2: Pearson correlation coefficients r and p, the critical r and level of significance values for the Mass parameters

Variables	r	p	Number of data points	critical r	significance
HI mass vs HI deficiency	-0.61	0.0003	30	0.463	0.01
Stellar mass vs HI deficiency	-0.03	0.87	22	0.360	0.1
Baryonic mass vs HI deficiency	-0.62	0.002	22	0.537	0.01
HI mass vs Stellar mass	0.37	0.087	22	0.360	0.05
Stellar mass vs V_{rot}	0.48	0.03	22	0.360	0.02
HI mass vs V_{rot}	0.07	0.76	22	0.360	0.1
Baryonic mass vs V_{rot}	0.34	0.34	22	0.360	0.1
A_{flux} vs HI mass	-0.24	0.22	28	0.317	0.1
A_{flux} vs Stellar mass	-0.18	0.44	22	0.360	0.1

4.1.3 Star formation rate

In this section, we explore the relation between the star formation rate and several other properties determined for the galaxies in our sample.

In general low mass galaxies have higher SFR or sSFR at more recent times than high mass galaxies, according to the downsizing scenario (Cowie et al. (1996)). Although we might expect lower values of SFR for higher mass galaxies, figure 4.17 and table 4.3 indicate that there is no such statistically significant trend in our sample. The higher mass galaxies have indeed a small SFR, but the low mass galaxies have a wide range of SFR.

SFR is indirectly related to the HI mass of a galaxy and higher HI content will potentially allow for more stars to form. In figure 4.18 there is a clear trend for SFR(UV) to increase with HI mass, Pearson r=0.79 with a level of significance=0.01 as seen in table 4.3 as was expected since HI is the underlying fuel for the star formation in galaxies.

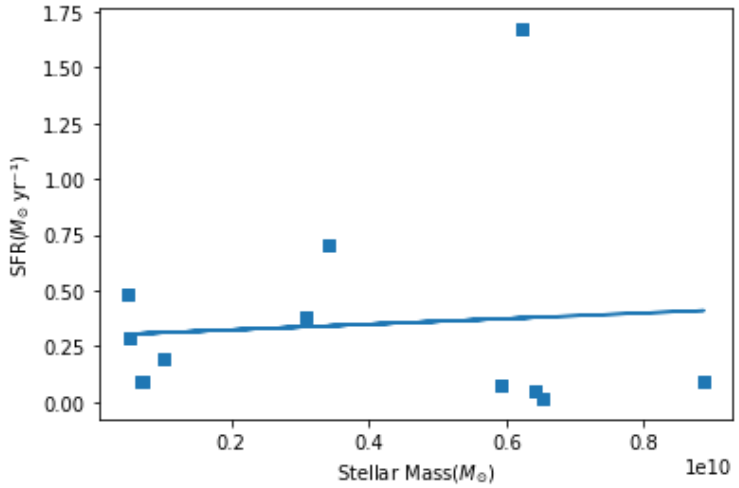

Figure 4.17: SFR(UV) as a function of the stellar mass. The blue line is the linear regression of the data.

Late type galaxies are expected to have higher SFR since they are in general rich in HI gas, then one would expect galaxies with larger values of SFR(UV) to have bluer colour, but figure 4.19 and the values of table 4.3 are not so conclusive even if the linear regression shows a slight tendency, Pearson r=0.39 with a level of significance=0.1 as seen in table 4.3, which is not statistically significant. But we can conclude that the redder galaxies seem to have very low SFR since no galaxy with a B-I colour >2 has a high SFR.

As discussed before, HI mass is expected to have a relation with the star formation rate because a galaxy with less HI than expected should have less capacity to create new stars.

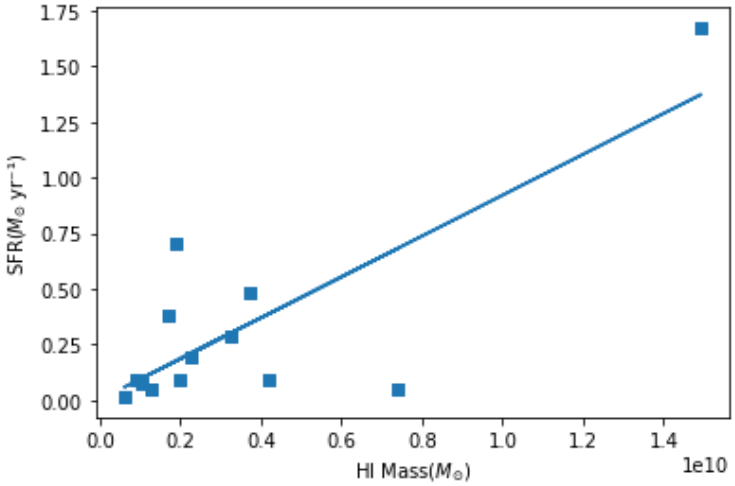

Figure 4.18: Star formation rate as a function of the HI mass. The blue line is the linear regression of the data.

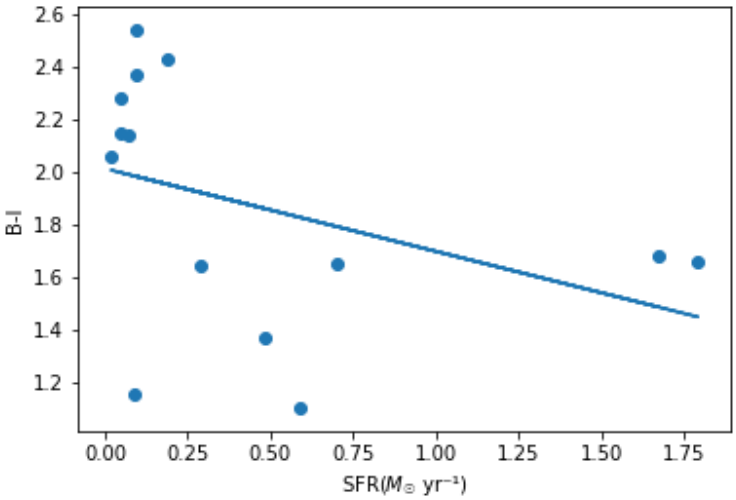

Figure 4.19: Relation between the colour(B-I) of the galaxies and their SFR(UV). The blue line is the linear regression of the data.

Therefore the HI deficiency should be an important factor for the SFR of the galaxies, since galaxies with a deficiency of HI will have lower SFR compared to galaxies with the same characteristics but without HI deficiency. In figure 4.20 we can see the galaxies with high HI deficiencies predominantly have very low SFR(UV)s, where as only the galaxies without deficiency or with excess HI content have a higher SFR(UV)s. Only one of the galaxies from our sample that has HI deficiency has a SFR not close to zero and its HI deficiency is very close to the threshold to consider it a galaxy HI deficient. Although the linear fit correlation r=-0.4 is not statistically significant we can conclude that high HI

deficiency is associated with lower SFR.

Regarding the A_{flux}, the relation to the SFR has a r=0.48, but because of the low number of galaxies in the sample with this data the relation is not statistically significant. Although there is a trend for the SFR to be lower with higher A_{flux} as seen in figure 4.21. Since we don't have any galaxy with a $A_{flux} > 1.26$ we can't make any definite conclusion from this plot. But galaxies with higher disturbances in their HI disk tend to have smaller SFR. This suggests a disturbance of the HI might be suppressing SFR in our sample.

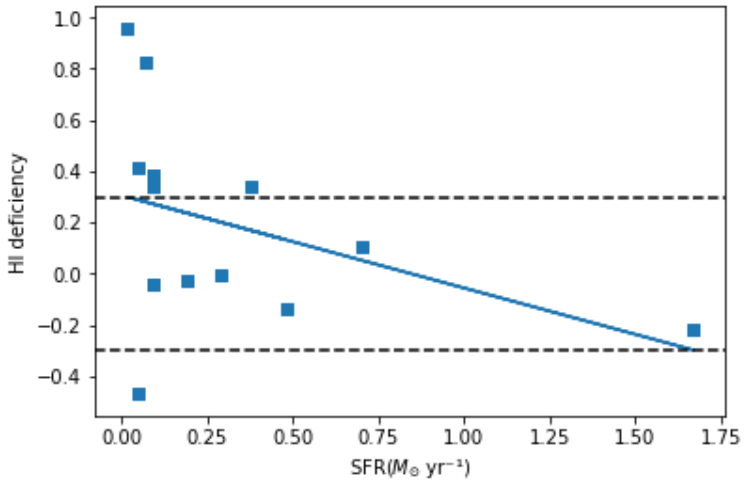

Figure 4.20: Relation between the HI deficiency and the star formation rate. Dashed lines at 0.3 and -0.3 indicate the values above and below which HI deficiency it's likely that the galaxies in fact have a HI deficiency or excess. The blue line is the linear regression of the data.

We can also explore the specific star formation rate, sSFR, which is the star formation rate of a galaxy divided by its stellar mass. This parameter allows us to compare more consistently high-mass with low-mass galaxies. In the nearby universe, the sSFR decreases for galaxies with higher stellar masses, massive galaxies formed their stars in the past whereas less massive ones are still quite actively star formation(as first evidenced by Cowie et al. (1996)), or equivalently, the mean age of the stellar populations of massive galaxies is higher than that of low mass galaxies.

In figure 4.22 we can observe galaxies with high sSFR tend to have lower stellar mass. In our data we see a trend in agreement with downsizing.

In figure 4.23, we expected galaxies with more HI mass to have a higher specific SFR, which we see is correlated r=0.57 with a level of significance=0.1.

For a more complete analysis on the specific star formation rate we analyse the correlation between the sSFR with HI deficiency and the A_{flux}.

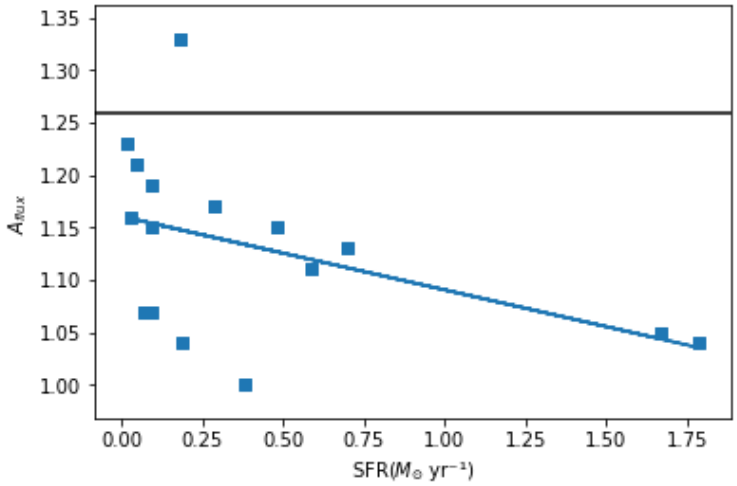

Figure 4.21: Relation between the A_{flux} and the star formation rate. The blue line is the linear regression of the data. The line at A_{flux}= 1.26 represents the value above which the HI profile asymmetry is likely reflecting an ongoing tidal or ram pressure interaction.

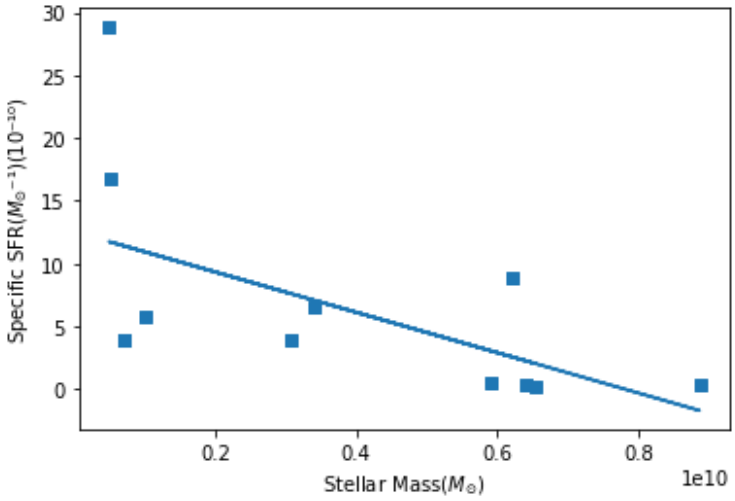

Figure 4.22: Specific star formation rate relation with the Stellar mass. The blue line is the linear regression of the data.

There is an expected relation between the HI deficiency with the specific star formation rate r=-0.397 as seen in table 4.3 is not statistically significant but there is a trend for galaxies with an HI deficiency to have a low specific SFR. Remarkably the relation of the HI deficiency with the SFR is very similar the specific SFR. But no clear trend between sSFR and A_{flux}, this implies that the galaxies in our sample with higher A_{flux} which are likely to be undergoing interactions do not show evidence that interactions are inducing

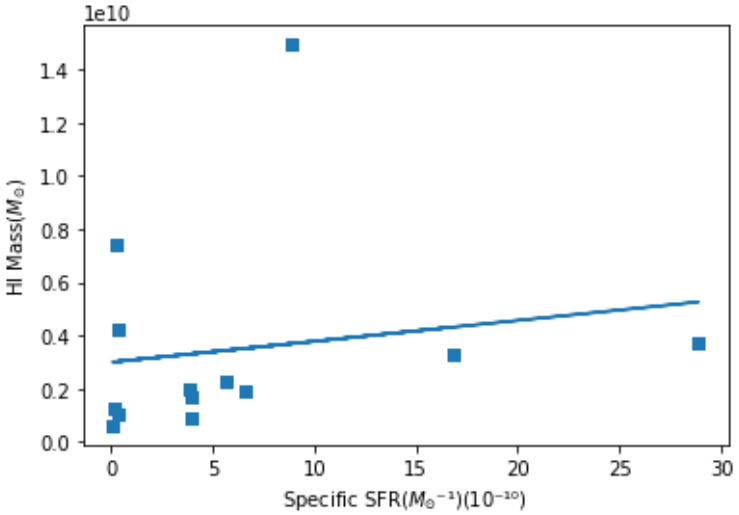

Figure 4.23: Specific star formation rate relation with the HI mass. The blue line is the linear regression of the data.

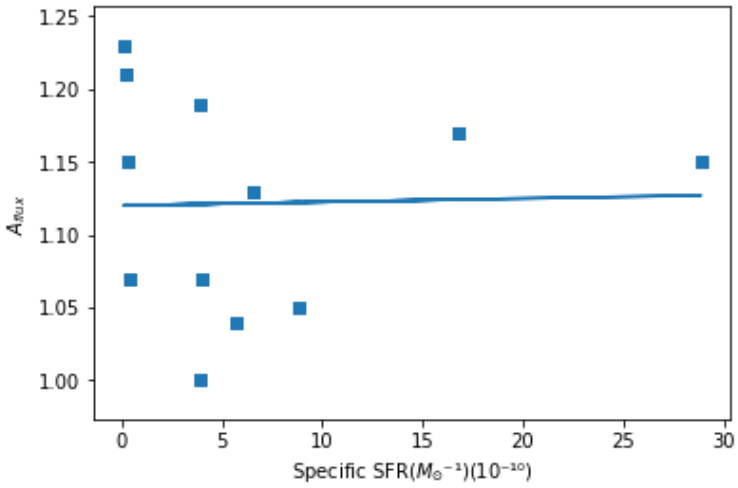

Figure 4.24: Specific star formation rate relation with the A_{flux}. The blue line is the linear regression of the data.

higher sSFRs. There are several models which predict enhanced SFR and sSFR from tidal and ram pressure stripping e.g. Kapferer et al.(2009). Although it should be noted that we have no sSFR data for galaxies with $A_{flux} > 1.26$ where the induced sSFR effect should be most evident.

In this section we showed the relation between the HI mass of the galaxies and their SFR, r=0.79 at a level of significance of 0.01. This correlation is weaker when we analyse

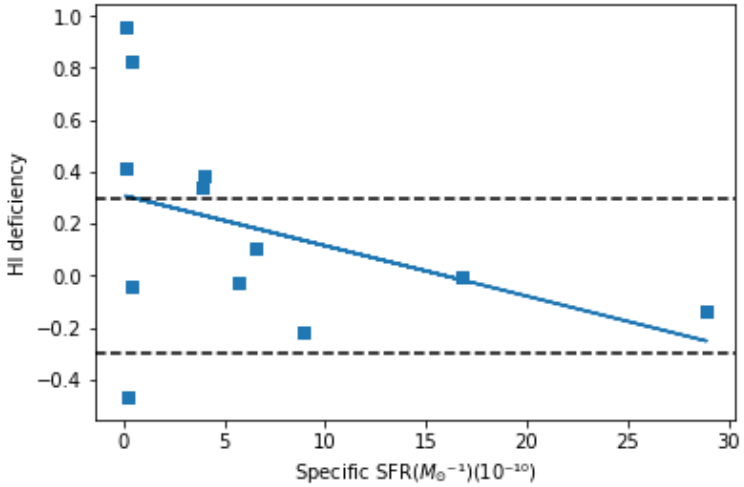

Figure 4.25: Specific star formation rate relation with the HI deficiency. The blue line is the linear regression of the data. Dashed lines at 0.3 and -0.3 indicate the values above and below which HI deficiency it's likely that the galaxies in fact have a HI deficiency or excess.

Table 4.3: Pearson correlation coefficients r and p, the critical r and level of significance values for the Star formation rate parameters

Variables	r	p	Number of data points	critical r	level of significance
Stellar mass vs SFR	0.08	0.8	12	0.497	0.1
HI mass vs SFR	0.79	0.001	13	0.684	0.01
Total Mass vs SFR	0.07	0.98	12	0.497	0.1
colour vs SFR	0.39	0.16	14	0.458	0.1
HI deficiency vs SFR	-0.4	0.17	13	0.476	0.1
A_{flux} vs SFR	-0.45	0.08	16	0.497	0.05
sSFR vs Stellar mass	-0.57	0.05	11	0.602	0.05
sSFR vs HI mass	0.57	0.04	13	0.476	0.1
sSFR vs HI deficiency	-0.397	0.18	13	0.476	0.1
sSFR vs A_{flux}	-0.14	0.66	12	0.497	0.1

the specific SFR with the HI mass, which gives a r=0.57 value with a level of significance of 0.1.

4.2 Comments on individual galaxies

In this section we analyse the galaxies with more extreme parameters and try to infer their history from the available data.

4.2.1 Galaxies with high A_{flux} values

The galaxies CGCG 522-006 and KUG 151+352 have an A_{flux} >1.26, these values allows us to conclude that their HI profile asymmetry is probably reflecting a tidal or ram pressure interaction.

CGCG 522-006(V_{HI} =5576 kms^{-1}), figure 4.26 is a face-on Sc galaxy, with optical inclination of 9 degrees as seen in table 2.1 with an A_{flux} = 1.27, above the threshold to consider that its HI disk is currently suffering an interaction. This galaxy has a HI excess of -0.399 dex and is located at 1864 kpc from the cluster centre.

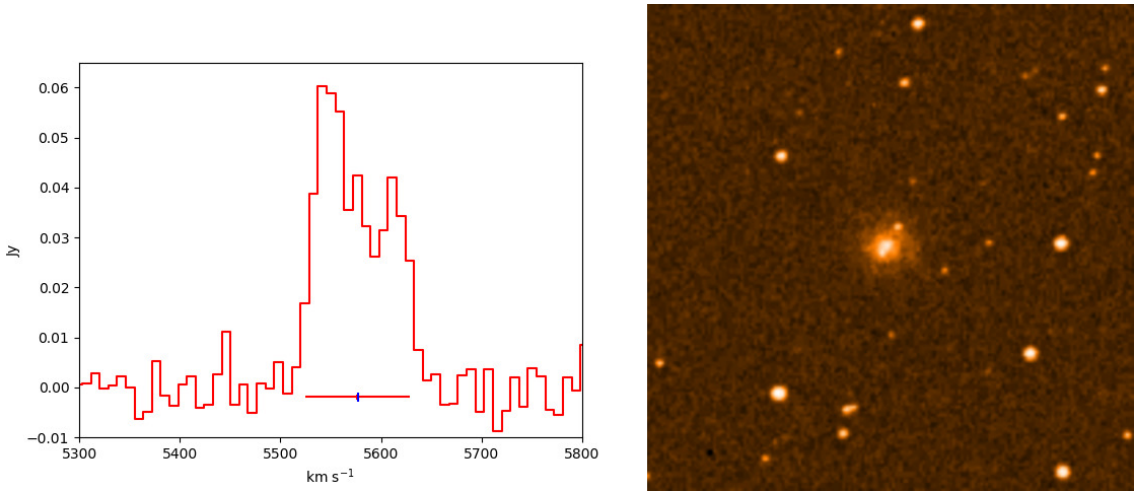

Figure 4.26: CGCG 522-006. Left panel shows a very asymmetrical HI profile, $A_{flux} = 1.27 \pm 0.08$. The right panel shows the optical image of the galaxy.

A NED search reveals the nearest companion is an Irr galaxy, CGCG 522-002(V_{HI} =5535 km s^{-1}) which is projected 16.6 arcmin(364 kpc) away. CGCG 522-006 is also close to CGCG 522-010(V_{HI} =5005km s^{-1} with a separation of 19.08 arcminutes). We don't have an available HI spectra for the companions. The HI spectra for CGCG 522-006 is very asymmetrical and the optical image shows a disturbance resembling a small tail. This is a indication of a tidal effect likely caused by an interaction with one of the companions that are close to it and at similar velocity. CGCG 522-002's DSS image appears disturbed, which suggest it's the most likely interaction companion for CGCG 522-006.

KUG 151+352 is a edge-on Sb galaxy with an optical inclination of 81 degrees, figure 4.27, and has a $V_{HI} = 5005 \pm 4 kms^{-1}$ with a A_{flux} of 1.33, with a low SFR of 0.18 $M_{\odot} yr^{-1}$ and a HI deficiency = 0.412 dex, which indicates that this galaxy is significantly HI deficient. KUG 151+352 galaxy is projected 40.8 arcmin(893 kpc) from the cluster center and located inside the 2σ of the virial radius obtained from Hassan et al.(2016). This

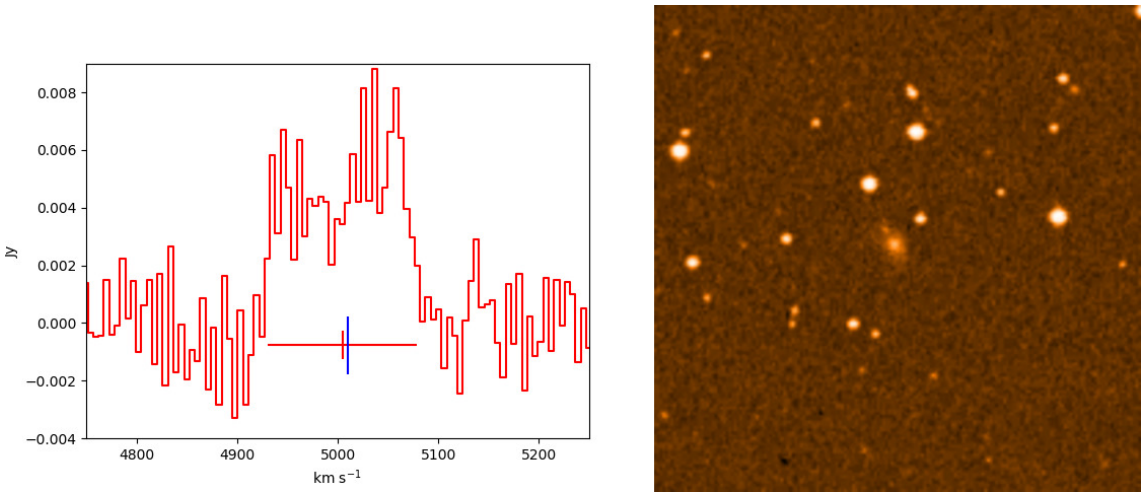

Figure 4.27: KUG 151+352. Left panel shows a asymmetrical HI profile, $A_{flux} = 1.33 \pm 0.04$. The right panel shows the optical image of the galaxy.

galaxy is a close companion to three other galaxies, the closest one being CGCG 522-060 with $V_{HI} = 4635 \pm 5 kms^{-1}$, with a separation of 11.78 arcminutes(258 kpc) and CGCG 522-060's optical morphology is clearly disturbed. The other galaxies with a separation below 25 arcminutes are CGCG 522-064 with $V_{HI} = 5531 \pm 1 kms^{-1}$ and LEDA 100158 with $V_{HI} = 4886 \pm 47 kms^{-1}$). For the CGCG galaxies we have a HI spectra since they are in our sample, but in the case of LEDA 100158 there is no available spectra. Both the CGCG galaxies that are close to KUG 151+352 have a $A_{flux} < 1.12$ which implies that their HI wasn't recently disturbed. In the case of KUG 151+352 there is a secondary peak in the optical image; this and the fact of this galaxy being relatively distant to the cluster center is a indication the KUG 151+352 may have recently accreted a satellite galaxy. On the other hand its high HI deficiency could be the result of earlier ram pressure stripping if the galaxy has previously transited the cluster core.

4.2.2 Analysing the galaxies with HI deficiency

The Sb galaxy CGCG 522-042 (see figure 4.28) has an HI deficiency of 0.95, this galaxy has the highest deficiency in our sample. It's at cluster centric distance 444 kpc and has

two close companions, LEDA 100151 and LEDA 197600 with a separation of 5.03 and 5.99 arcmin, respectively. It has a A_{flux}=1.23 and the optical image shows a slightly disturbed disk. Given the proximity to the cluster center and high HI deficiency it seems most probable ram pressure stripping is the primary cause of the HI deficiency, with the low A_{flux} indicating this stripping occurred some time ago.

The SBc galaxy UGC 1366 (see figure 4.31) has also a high HI deficiency of 0.825 dex with a high A_{flux}=1.07 and its optical image shows a galaxy with no disturbance on its disk. It's at cluster centric distance 697 kpc and has two close companions,CGCG 522-049 and LEDA 2081954 with a separation of 7.047 and 7.243 arcminutes, respectively. This galaxies does not have a available HI spectra.

The Sb galaxy CGCG 522-071 (see figure 4.29) has also a high HI deficiency of 0.895 with a high A_{flux}=1.21 and its optical image shows a galaxy with a slight disturbance on its disk. It's at a cluster centric distance of 816 kpc without any close companions. This implies that this galaxy had been striped of its HI content a long time ago and probably this HI deficiency was caused by ram-pressure stripping. Due to the low signal to noise ratio of the HI profile of this galaxy was not included.

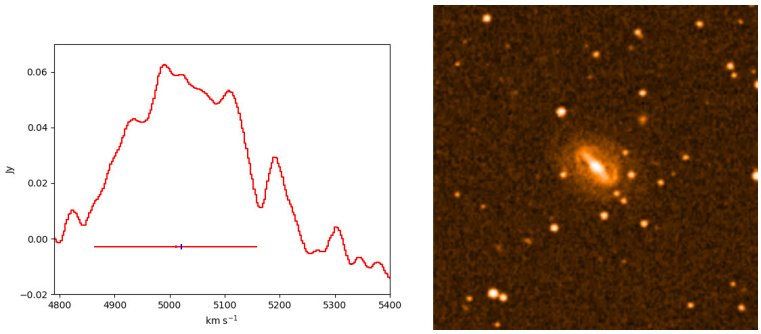

Figure 4.28: CGCG 522-042. Left panel shows a asymmetrical HI profile, $A_{flux} = 1.23 \pm 0.17$. The right panel shows the optical image of the galaxy.

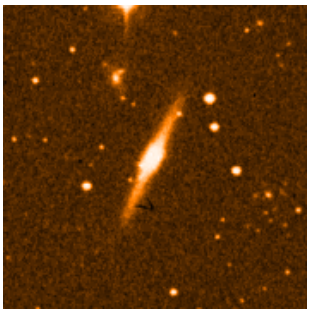

Figure 4.29: CGCG 522-071. Optical image of the galaxy. $A_{flux} = 1.21 \pm 0.11$

The E-S0 galaxy CGCG 522-046 (see figure 4.30) is a galaxy with an HI excess and even with this HI excess, it has a very low SFR. This behaviour remains when we explore the relation between the HI deficiency with the specific SFR. This galaxy is rich in HI gas but seems unable to efficiently form stars. It's most likely the HI deficiency reflects the galaxy being an early type and the HI could have been accreted during an interaction with a gas rich neighbour. The galaxy CGCG 522-086 is the galaxy with the highest HI excess from our sample, but since we don't have access to this galaxy FUV flux we couldn't calculate its SFR.

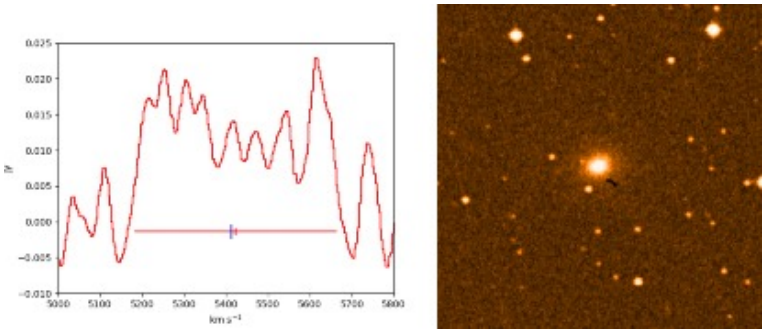

Figure 4.30: CGCG 522-046. Left panel shows a asymmetrical HI profile, $A_{flux} = 1.21 \pm 0.09$. The right panel shows the optical image of the galaxy.

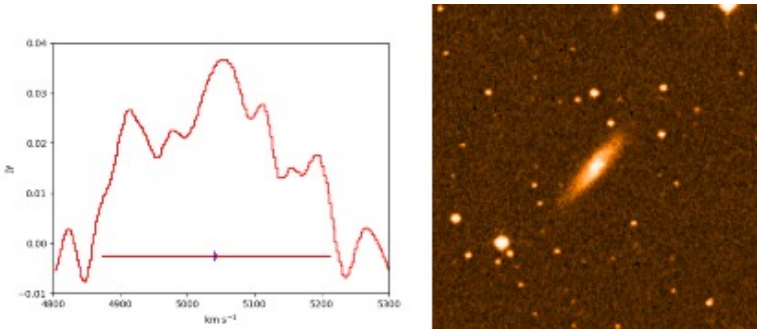

Figure 4.31: UGC 1366. Left panel shows a symmetrical HI profile, $A_{flux} = 1.07 \pm 0.02$. The right panel shows the optical image of the galaxy.

4.2.3 Analysing galaxies with higher SFR

The galaxy CGCG 522-001 (see figure 4.32) and CGCG 522-020 (see figure 4.33) have the highest SFR from our sample with a projected distance of 1620kpc and 1174kpc respectively. In case of CGCG 522-020, it has an average stellar mass and does not have an HI deficiency (-0.22) and its optical images shows a disturbed disk. In case of CGCG 522-001 there is no HI deficiency (-0.199) and doesn't show any optical disturbance. CGCG

522-001 doesn't have an available K-band magnitude available so we are unable to calculate its stellar mass. CGCG 522-020 has a high SFR 1.67 $M_{\odot}yr^{-1}$ which is consistent with $M_{HI}(1.4\times10^{10}solarmasses)$ which is the highest in our sample. For CGCG 522-001 $A_{flux}<1.05$ so there is no evidence that the SFR was induced by a recent interaction perturbing his HI. It's optical image appears undisturbed, so it SFR appears to be attributable to the large reservoir of gas. CGCG 522-020 optical image is less symmetric so the SFR may be the result of a tidal interaction and with an $A_{flux}<1.05$ it has some features which would be consistent with a recent interaction which may have induced the high SFR.

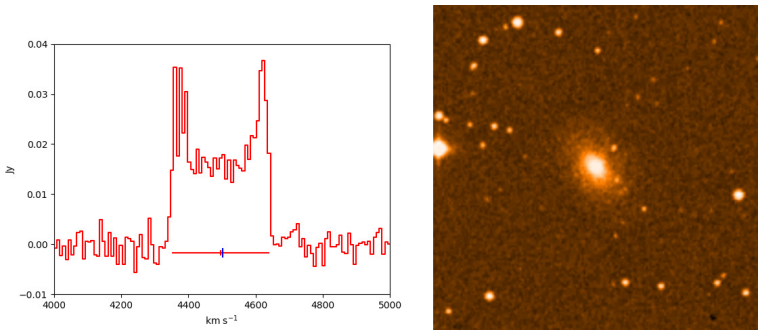

Figure 4.32: CGCG 522-001. Left panel shows a symmetrical HI profile, $A_{flux}=1.04\pm0.04$. The right panel shows the optical image of the galaxy.

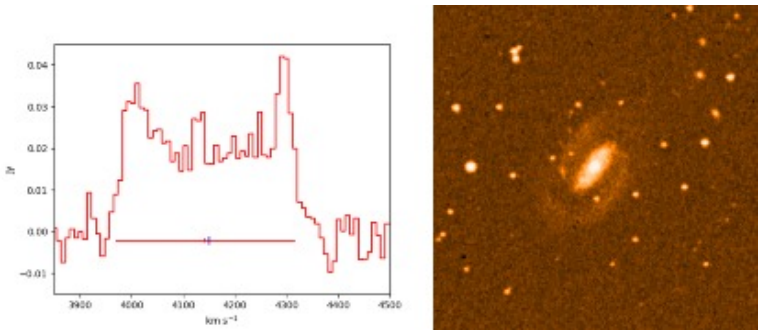

Figure 4.33: CGCG 522-020. Left panel shows a symmetrical HI profile, $A_{flux}=1.05\pm0.1$. The right panel shows the optical image of the galaxy.

CGCG 522-038 (see figure 4.35) was studied previously by Bravo et al.(1997). Who obtained a resolved map of the HI of this galaxy. As seen in figure 4.34, this galaxy shows a disturbance in its HI disk but the A_{flux}=1.13 we obtained which doesn't reflect this perturbation. This galaxy has no HI deficiency according to our data and is in agreement with the data from Bravo et al.(1997) which also states that this galaxy has no deficiency. This galaxy has one close companion, CGCG 522-018 which is part of our sample. It has a $A_{flux}=1.11$, no HI deficiency and a disturbed optical disk. According to Bravo et al.(1997)

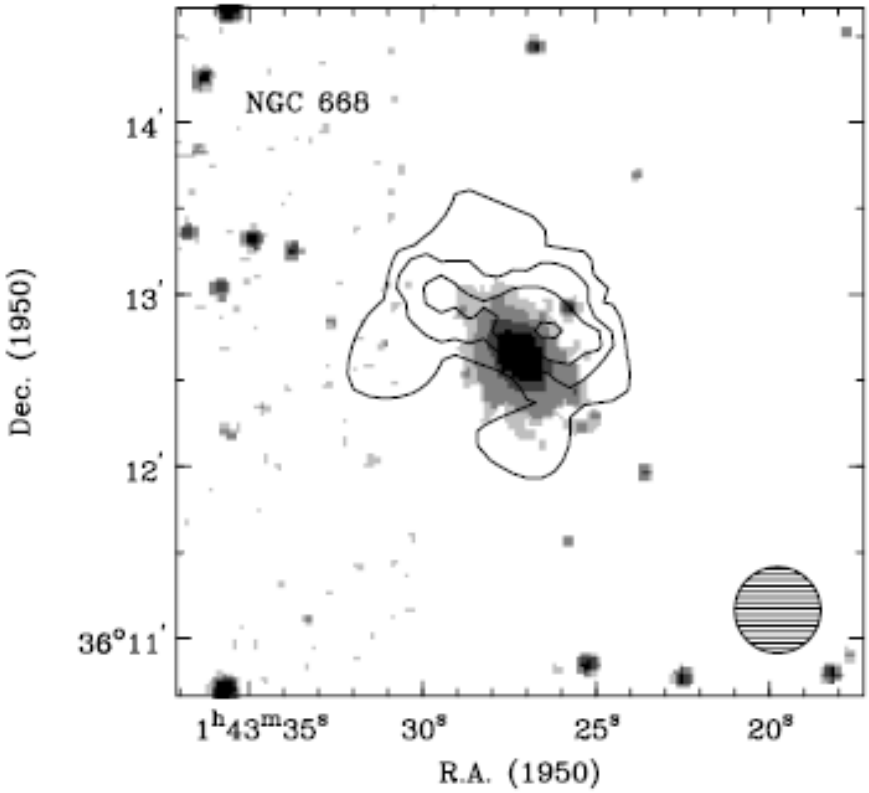

Figure 4.34: HI density distribution of CGCG522-038. Image obtained from Bravo et al.(1997)

the asymmetry of one of the arms of CGCG 522-038 is pointing towards CGCG 522-018 but the separation between this galaxies is considered to be to much for this galaxies to be interacting. The irregular HI morphology of this galaxy can be explained by tidal effects which might have caused during this interaction.

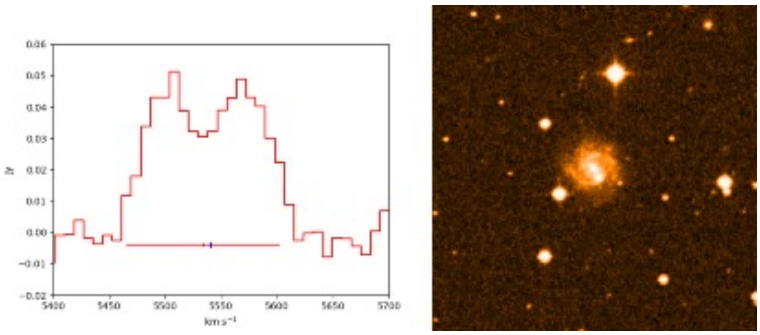

Figure 4.35: CGCG 522-038. Left panel shows a symmetrical HI profile, $A_{flux} = 1.13 \pm 0.01$. The right panel shows the optical image of the galaxy.

The detailed considerations of galaxies with extreme properties rarely allows for a

definitive conclusion about the cause of these extreme properties but seems to point toward a mix of tidal and ram pressure mechanisms. In the one case where we have resolved HI the A_{flux} parameter don't reflect the perturbation of HI revealed in the HI map. Also the low resolution and depth of the available DSS images made assessment of the presence of tidal features difficult. A higher quality imaging survey would significantly help in determining the interaction mechanisms at play in these galaxies.

Chapter 5

Conclusion

In this work we analyzed parameters from 30 galaxies that belong to the cluster Abell 262 within a velocity range of 4428 to 5276kms^{-1}, of which 28 galaxies have HI spectra available and 2 only having upper limits for their HI detection. We were able to calculate stellar masses for 22 and star formation rate for 17 of the sample galaxies.

The HI deficiency is related to the distance from the cluster center as was expected, in the sense that galaxies tend to be more HI deficient when they are located closer to the cluster center, with a Pearson r coefficient of -0.32 with a level of significance of 0.1 for this relation. This behaviour of the galaxies of our sample can be explained by stronger ram pressure stripping and/or higher frequency of tidal harassment interactions near the cluster center. Abell 262 is a cluster with low X-ray emission from the cluster ICM, indicating an ICM density which is less capable of stripping HI gas from the galaxies, this characteristic explains the low correlation between these parameters when compared to clusters with higher X-ray emissions, e.g. the Coma cluster.

The Tully-Fisher relation for the stellar mass(TFR) and for the baryonic mass(BTFR) had Pearson correlation coefficients of 0.48 and 0.34 respectively. The respective levels of confidence were 0.02 and 0.1. For BTFR the smaller r value implies that the cluster environment is causing a divergence from this normally tight relation probably by HI removal and disturbing the HI kinematics. No relation was found between the A_{flux} and the HI deficiency, we hypothesise that galaxies with a high A_{flux} are currently being stripped of their gas and as the HI stripping progresses, this galaxies will gain an HI deficiency and the HI disk will eventually return to equilibrium. Showing then a lower A_{flux} and high HI deficiency. The star formation rate was calculated for only 17 galaxies because of the absence of a far-UV flux. But we were able to still get correlation between the

HI mass and the SFR with a Pearson correlation coefficient of 0.79 which corresponds to a level of significance 0.01. Looking at the individual galaxies only two show clear signs of recent HI striping caused by environmental effects from their A_{flux} values, CGCG 522-006(A_{flux}=1.27) and KUG 151+352(A_{flux}=1.33). In the case of CGCG 522-006 probably tidal effects from an interaction with a nearby companion caused this disturbance of the HI disk due to the asymmetrical HI spectra of this galaxy and a visible disturbance in its optical image. For KUG 151+352 given its projected distance from the cluster(893 kpc) it A_{flux} is likely due to the recent accretion of a satellite indicated in its optical image but we can't rule out the possibility that this could be a result from ram pressure stripping if the galaxy had previously transited the cluster core. CGCG 522-042 shows a very high HI deficiency which is possibly caused by tidal effects but given it projected proximity to the cluster core(444 kpc) is more likely due to past ram pressure stripping. UGC 1366 and CGCG 522-071 also show very high deficiency(0.89) but in these cases the low A_{flux} and projected distances from the cluster center suggest past ram-pressure stripping as the cause of this deficiency. Analysing the SFR of the galaxies from our sample the galaxy CGCG 522-020 doesn't have a HI deficiency(-0.22) and has a very high HI content which reflects in a very high SFR, this galaxy shows a disturbed stellar disk, we hypothesised that this galaxy had an tidal interaction which is triggered to the enhance SFR. The galaxy CGCG 522-038 which was previously mapped in HI by Bravo et al.(1997) shows a disturbed HI and optical disks which suggests a possible tidal interaction with another galaxy. The $A_{flux} = 1.13$ implies that this interaction didn't happen recently but the interferometric HI show a clear disturbed HI. The optical images helped us understand possible disturbances in the optical disk but a disturbance which together with disturbed HI is clear sign of tidal interaction. This case show that interferometric mapping is more sensitive to interactions impacting HI than A_{flux}, where the HI surface density is overlaid on i-band image.

We showed that it's possible to gain insights into the processes galaxies are undergoing and environmental effects that happened in their past thanks to their HI spectra and optical data. The HI content of the galaxies can give a glimpse of the galaxies past and present but the results can be inconclusive. With spacial data about the HI disk of the galaxies from our sample we could have more detailed understanding of their evolutionary histories and the impact of the cluster environment. The HI surface density mapping would help us to know how the HI is distributed inside galaxies and a comparison between this and the optical image of the galaxies will allow to determine which processes could have cause HI

stripping.

Bibliography

Bravo-Alfaro, H.; Szomoru, A.; Cayatte, V.; Balkowski, C.; Sancisi, R., 1997, A&AS, 126, 537 [Cited on pages 47, 48, and 52.]

Broeils A. H., Rhee M., 1997, AA, 324, 877 [Cited on page 5.]

Cardelli, A.J., 1989, ApJL, 345, 245-256 [Cited on page 21.]

Clowe, D., M. Brada c, A. H. Gonzalez, M. Markevitch, S. W. Randall, C. Jones, and D. Zaritsky. 2006 ApJL, 648:L109–L113 [Cited on page 2.]

Cowie et al., AJ 112, 839 [Cited on pages 37 and 39.]

Espada.D. et al,. 2011, A&A, 532, 117 [Cited on pages 19 and 27.]

Fadda, T. et al., 1996, ApJ v.473, p.670 [Cited on pages 3, 4, and 26.]

Gavazzi, G,. 1989, ApJ, 346, 59 [Cited on pages xi, 18, and 26.]

Gunn, James E.; Gott, J. Richard. 1972, ApJ, 176, 1 [Cited on pages 6 and 7.]

Haynes, P,. et al. 1984, ARAA, 22,445 [Cited on page 17.]

Hassan, M.S.R. 2016 MNRAS 458, 264-269 [Cited on pages 3, 4, 11, 26, and 44.]

Holwerda B. et al., 2011 MNRAS 416, 2401-2414 [Cited on page 26.]

Jáchym, P,. et al,. 2019, ApJ, 883, 145 [Cited on page 7.]

Jog, C,. Combes, F,. 2008, Phys. Rep. 471, 75-111 [Cited on page 5.]

Kapferer. 2009, AA, 499, 87-102 [Cited on pages 8, 9, and 41.]

Kemicutt,Robert C. 1998 ApJ, 498, 541-552 [Cited on page 5.]

Kravtsov, A. V., Borgani, S., 2012, ARAA, 50, 353 [Cited on page 1.]

Kron, R.G., 1980, ApJS, 43, 305 [Cited on page 21.]

Lee, C., 2009, ApJ, 706, 599 [Cited on page 22.]

Lewis, I,. 2002, MNRAS, 334, 3, 673-683 [Cited on page 2.]

Neill, D., 2001, Apj, 548, 550 [Cited on pages 3, 4, and 26.]

Plionis, M., Tovmassian, H. 2003, AA, 416, 2, 441-446 [Cited on pages 2 and 3.]

Román, J., Trujillo, I,. 2017, MNRAS, 468, 703 [Cited on page 1.]

Schlafly, E. Finfbeiner, D.P.,. 2011, AAS, 43 [Cited on page 21.]

Sengupta et al,. 2013, MNRASL 431, L1–L5, 1 [Cited on pages xi and 9.]

Skrutskie, 2006, AJ, 131, 1163 [Cited on page 20.]

Solanes, M. et al., 2001, ApJ, 548, 97 [Cited on pages 13, 17, and 18.]

Springob, M,. et al. 2005, ApJ, 621, 215 [Cited on pages 11 and 17.]

Scott, T.,. et al. 2010, MNRAS, 403, 3, 1175-1192 [Cited on page 8.]

Watts, AJS 105 [Cited on page 27.]

Wang J. et al., 2017, MNRAS, 472, 3029 [Cited on page 6.]

Wegner, 1993, AJS 105 [Cited on page 11.]

Wen, Q., Wu, H., Zhu, Y., 2013, A&AS, 126, 537 [Cited on page 21.]

Willmer C.N,A., 2018, ApJS, 236, 47 [Cited on page 21.]

Wu, Xiang-Ping, C. Tzihong, F.Li-Zhi, 1998, MNRAS, 301, 861 [Cited on pages 2 and 3.]

McGaugh et al. ApJ 533, 99 [Cited on page 31.]